Implications of surfactant hydrophobic chain architecture on the Surfactant-Skin lipid model interaction

Yao Chen, Mingrui Liao, Kun Ma, Zi Wang, Bruno Demé, Jeff Penfold, Jian R Lu, John R. P. Webster, Peixun Li

Published version information

Citation: Y Chen et al. Implications of surfactant hydrophobic chain architecture on the Surfactant-Skin lipid model interaction. J Coll Int Sci 608 (2022): 405-415

Implications of Surfactant Hydrophobic Chain Architecture on the Surfactant-Skin Lipid Model Interaction

Yao Chen[1], Mingrui Liao[2], Kun Ma[1], Zi Wang[3], Bruno Demé[4], Jeff Penfold[1], Jian R Lu[2], John R. P. Webster[1] and Peixun Li[1,†]

[1] ISIS Facility, Rutherford Appleton Laboratory, STFC, Didcot, OXON, UK, OX11 0QX

[2] Department of Physics & Astronomy, the University of Manchester, Manchester, M13 9PL, UK

[3] School of Science, State Key Laboratory of Heavy Oil Processing, China University of Petroleum , Qingdao 266580, China

[4] Institut Laue-Langevin, Grenoble, France

[†] **Corresponding Author:** Peixun Li, email: peixun.li@stfc.ac.uk

Key words: skin lipids, stratum corneum, cationic surfactants, neutron diffraction, membrane hydration, permeability

TOC:

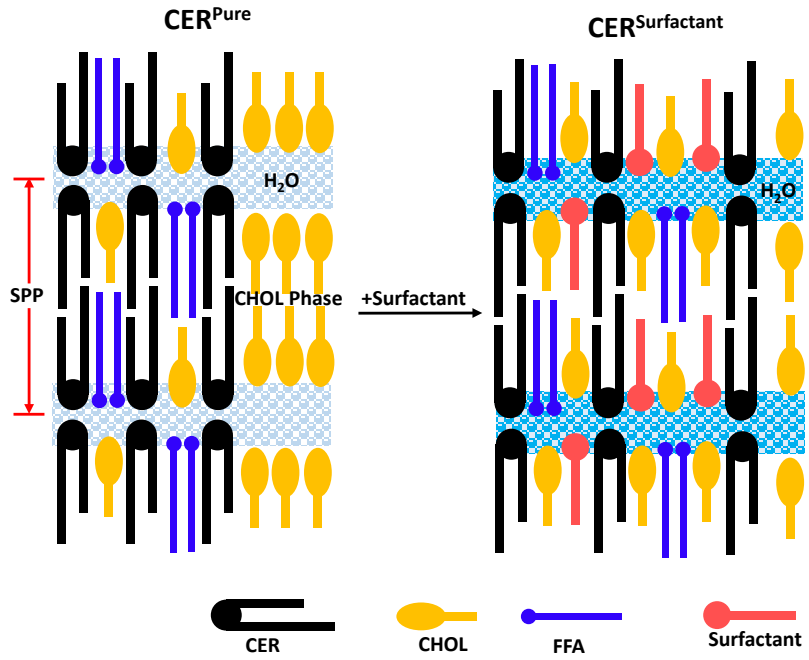
CER^Pure
CER^Surfactant
H2O
H2O
SPP
CHOL Phase
+Surfactant
CER
CHOL
FFA
Surfactant

ABSTRACT

Although surfactants have been widely used in skin care and other related applications, our knowledge about how surfactants interact with stratum corneum (SC) lipids remains limited. This work reports how surfactants interact with a lipid SC model by neutron diffraction and molecular dynamics (MD) simulations, focusing on examining the impact of surfactant molecular architecture. The surfactant-SC mixed membrane was constructed by an equimolar mixture of ceramide/cholesterol/fatty acids and surfactant at 1% molar ratio of total lipids. The arrangements of water and surfactant molecules in the membrane were obtained through neutron scattering length density (NSLD) profiles via contrast variation method, meanwhile, MD simulation clearly demonstrated the mechanism of hydration change in the surfactant-model SC mixed membrane. No drastic difference was detected in the repeating distance of the short periodicity phase (SPP) upon adding surfactants, however, it significantly enhanced the membrane hydration and reduced the amount of phase separated crystalline cholesterol, showing a strong dependence on surfactant chain length, branching and double bond. This work clearly demonstrates how surfactant architecture affects its interaction with the SC membrane, providing useful guidance for either choosing an existing surfactant or designing a new one for surfactant-based transdermal application.

1. INTRODUCTION

Skin is fast becoming a target of drug delivery via various transdermal routes that are mostly non-invasive and that can be self-administrated, thus improving patient compliance and sustaining drug release for long periods of time.[1] The greatest challenge for transdermal delivery is that only a limited number of drugs are amenable to dermal administration. Stratum corneum (SC) provides a barrier to protect the skin from desiccation and external molecules, and so restricts the design of transdermal drug delivery vehicles.[2] As the outermost layer of human skin, the SC consists of dead keratin-filled corneocytes that are surrounded by the crystalline lamellar lipid matrix to form a brick-and-mortar structure.[3] The 'brick', corneocyte, was initially thought to be impermeable, but evidence from the diffusion of drugs through corneocytes proved opposite.[4-6] However, the rate-limiting factor for the permeability of SC is still the lipid matrix which exists continuously whilst the corneocytes do not.

Interaction between drug carrier and lipid layers could change the lipid packing in SC, resulting in the enhancement of skin permeability. Surfactants have been extensively investigated in drug delivery as drug carrier due to their superior amphiphilicity and self-aggregation properties.[7] Meanwhile, studies have suggested that suitable combination of surfactants with other enhancers may offer a balance between enhancement and irritation.[1, 8] Therefore, interactions between surfactants and skin-barrier lipids are of great importance to understand the strategy to target surfactants as drug carriers and chemical enhancers for transdermal delivery.

The human skin lipid matrix is mainly composed of ceramides (CERs), cholesterol (CHOL) and free fatty acids (FFAs). The CERs typically contain a long acyl chain linked to a sphingoid base through an amide linkage. The structural variation of acyl chain and sphingoid base leads to a broad diversity of CERs, and approximately 17 subclasses of CERs have been

identified in human skin.[9-10] FFAs with chain length from C16 to C26 have been found in SC, among which C22 and C24 acids dominate. The structures of the lipid matrix have been extensively probed using X-ray diffraction,[11] neutron diffraction,[12-15] infrared spectroscopy,[16-17] and electron microscopy.[18] Due to the structural difference of CERs, especially the acyl chain length and mobility of ceramide, two repeating units are formed in SC, including the short periodicity phase (SPP) with repeating distance of ~ 6 nm and the long periodicity phase (LPP) with repeating distance of ~ 13 nm.[19] The electron density profiles obtained from the X-ray diffraction measurements for CERs/CHOL/FFAs mixtures indicate a bilayer arrangement for SPP and a multilayer structure for LPP, respectively.[20] The most acceptable structure of LPP is a sandwich model with two crystalline bilayers surrounding a fluid centre.[21] In recent years, Bouwstra et al.[12-15] systermatically explored the lipid molecular arrangements in the unit cell of SPP and LPP by neutron diffraction. Meanwhile, the interactions between model phospholipid (dipalmitoylphosphatidylcholine, DPPC) and SC lipids were also invetigated.[17] Moreover, simulation studies using molecular dynamics (MD) were used to probe more detailed structures of SPP and LPP.[22-25] Eric et al.[23] proposed the mechanisms of unique lipid conformational transitions during LPP formation and the diffusion process of small molecules such as ethanol. Hoopes et al.[26] found that the addition of 0 ~ 0.1 mol % of oleic acid in the model SC (SPP) could enhance cholesterol diffusion. The ultimate goal of studying the SC structure and its interaction with topical enhancers is to provide guidance for the development of transdermal drug delievery. However, to the authors knowledge, very limited infromation has been reported about the interaction between long-chain cationic surfactant and model SC lipids even though these surfactants are potentially useful drug carriers and penetration enhancers.

Unlike previous work studying the interaction of surfactant monomeric and micellar solution with SC lipids,[27-29] this work explores the interactions of cationic surfactants with

model SC membrane in the condensed phase. Here, we focus on whether surfactants could manipulate the nanostructure of model SC membrane. Four surfactants with various architectures of hydrophobic chains were employed (*R*-HAB), i.e., cetyl bis(2-hydroxyethyl)-methylammonium bromide C_{16}HAB, oleyl bis(2-hydroxyethyl)-methylammonium bromide OHAB, stearyl bis(2-hydroxyethyl)-methylammonium bromide C_{18}HAB and isostearyl bis(2-hydroxyethyl)-methylammonium bromide IHAB. It is known that the hydrophobic chain fluidity of surfactant influences its performance as chemical enhancer in drug delivery.[1, 7, 30-31] The strategy for varying the chain fluidity is to adjust the hydrophobic chain architecture, such as changing the chain length and incorporating branched or unsaturated covalent bonds into the alkyl tail. This enables superior self-assembly ability as well as lower Kraft point to the surfactants. Comparing with the complex lipid mixtures mimicking the real SC composition in former studies, a simple system containing one ceramide and two fatty acids was used in this work to construct the model membrane. Neutron diffraction experiments were performed to determine the model membrane structure, followed by characterizing the impact from surfactant binding. Neutron scattering length density (NSLD) profiles and molecular dynamics (MD) simulations were performed to understand the mechanistic processes underlying the surfactant-model SC membrane interactions.

2. EXPERIMENTAL SECTION

2.1. Materials

Cationic ammonium surfactants oleyl bis(2-hydroxyethyl)-methylammonium bromide OHAB, stearyl bis(2-hydroxyethyl)-methylammonium bromide C_{18}HAB, isostearyl bis(2-hydroxyethyl)-methylammonium bromide IHAB and cetyl bis(2-hydroxyethyl)-methylammonium bromide C_{16}HAB were synthesized and purified according to the reported procedures.[32-34] No minimal point was found in the surface tension curves (Figure S1), which indicates the high purity of the surfactants. N-lignoceroyl-D-erythro-sphingosine CER NS (C24) was purchased from Avanti Polar Lipids, Inc. Cholesterol, behenic acid (C22) and lignoceric acid (C24) were obtained from Sigma Aldrich. Ceramides, cholesterol and fatty acids were used without further purification. Deuterium dioxide was purchased from Sigma Aldrich. The silicon wafer was obtained from Si-Mat (Kaufering, Germany). All organic solvents (analytical grade) were provided by Sigma Aldrich and used as received. High purity water (ElgaUltrapure with a resistivity of 18.2 MΩ·cm) was used in all the experiments.

2.2. Composition of the model lipid mixtures and sample preparation

Five types of model lipid membranes were constructed in this study. Their name, composition, and molar ratios are shown in Table S1. Pure ceramide mixture (CER^{Pure}) was made by an equimolar mixture of ceramide, cholesterol and fatty acid, among which the fatty acid was an equimolar mixture of C22 acid and C24 acid. To investigate the lipid-surfactant interaction, surfactant at a 1.0 % molar ratio of the total lipid was added to the lipid mixtures during sample preparation. For selected surfactant, the surfactant concentration was increased to 2.0 % molar ratio of the total lipids to evaluate the impact of concentration.

The sample preparation method and equilibration procedure were similar to those described previously.[12, 15] For each model membrane, the appropriate portions of lipids and surfactants were dissolved in a methanol/chloroform (1:2 v/v) mixture at a total concentration

of 10 mg/mL. Subsequently, this mixture was sprayed on the silicon surface by the "rock and roll method" within an area of 2.0 × 2.1 cm^2. The solvent was removed by a gentle flow of nitrogen. In total, ~ 5.0 mg of lipids and surfactants were sprayed on the silicon substrate.

After removing the solvent under vacuum, the sample was equilibrated at ~ 70 °C for half an hour and then cooled down to room temperature. Afterwards, the sample was hydrated with D_2O/H_2O buffer under 90% relative humidity (RH) at 32 °C for ~ 8 h. The humidity was controlled in a customized humidity chamber designed by ILL (the Institute Laue-Langevin). For each sample, three D_2O/H_2O volume ratios (8:92, 50:50 and 100:0) were used to hydrate the sample before the neutron diffraction experiments. The hydration time for the same sample between two measurements was ~ 8 h.

2.3. Surface tension measurements

The surface tension changes of all the surfactants in aqueous solution were measured with a Kruss K100 maximum pull tensiometer with a platinum plate. The time-dependent changes were followed at 25.00 ± 0.01 °C until successive values agreed to within 0.1 mN/m. All the surface tension curves were repeated three times or more and the values plotted were averaged.

2.4. Neutron diffraction experiments

Neutron diffraction experiments were performed on the D16 cold neutron diffractometer at ILL in Grenoble, France. The neutron wavelength of λ = 4.48 Å was generated by the reflection from a highly ordered pyrolytic graphite (HOPG) monochromator. During the experiment, the sample angle ω was rotated in a ω-scan with a fixed detector position. The intensity of the scattered neutrons was recorded by a two-dimensional ^{3}He detector as a function of scattering angle 2θ. The sample to detector distance is 955 mm. The area of the position-sensitive detector is 320 mm × 320 mm, with a spatial resolution of 1 mm × 1 mm. To maintain a constant temperature and relative humidity, the sample was mounted on a

goniometer in a lockable aluminum humidity chamber. The sample temperature was fixed at 32 °C for all the measurements, the physiological skin temperature. While measuring a sample at certain hydration level, the same D_2O/H_2O mixture was added into the chamber to keep a constant 90% RH. The measuring time varied from 4 ~ 6 h, depending on the signal-to-noise ratio.

2.5. Neutron data analysis

Water calibration measurement was made to correct for the efficiency of the detector. The background measurement was made by measuring the empty chamber, which was subtracted from experimental data to improve the signal/noise. The ILL in-house software package LAMP was used to reduce and normalise the data.[35] The 2D data was integrated in the vertical direction to a 1D curve and plotted as scattering intensity against scattering angle (2θ). The scattering angle is converted to the scattering vector q by:

$$q = \frac{4\pi \sin\theta}{\lambda} \quad (1)$$

where, λ is the neutron wavelength, θ is the Bragg angle. The repeat distance (d) of the lamellar phase for the model membrane is calculated by:

$$d = \frac{2\pi h}{q_h} \quad (2)$$

Here, h is the diffraction order. During the neutron diffraction measurements, the sample was rotated in steps of 0.05° from -1° to 20° to cover all the diffraction peaks. For each diffraction order, the high intensity peaks around the Bragg order position were integrated. Five scans near the Bragg angle in a total ω range of 0.2° (ω = -0.1, -0.05, 0, 0.05, 0.1) were selected and integrated. The integrated peaks were fitted with Gaussian:

$$f(x) = ae^{-\frac{(x-\mu)^2}{2\sigma^2}} + c \quad (3)$$

Where a is the intensity of peak, μ is the peak position, σ is the standard deviation and c is the offset for the baseline correction. The Gaussian peak height (I_h) was obtained from the fitting

curve, which was used to calculate structure factor amplitude ($|F_n|$):

$$|F_h| = A_h\sqrt{L \cdot I_h} \quad (4)$$

L is the Lorentz correction; the value was calculated by the $\sin 2\theta$ value. A_h represents the sample adsorption correlation factor, and was calculated as follows[36]:

$$A_h = \frac{1}{\sqrt{\frac{\sin\theta}{2\mu l}\left(1-e^{\frac{-2\mu l}{\sin\theta}}\right)}} \quad (5)$$

Here, l is the thickness of the sample and μ is the linear attenuation coefficient. The calculated sample thickness is 15 μm according to the reported methods.[12, 15] In brief, the total amount of lipids, the sprayed area and lipid density were combined to get the lipid thickness. The attenuation coefficient was obtained by using the lipid film density, chemical composition and neutron wavelength.

It is reported that the unit cell of SPP is a centrosymmetric arrangement, which means that the phase signs of structure factors could be either 0 or π. Therefore, the amplitudes of the structure factors linearly change with the D_2O/H_2O ratio.[36-37] Assuming the water molecules being located at the boundary of the unit cell this gives a phase sign distribution of – + – + – for the five diffraction orders. Additionally, the structure factor for the water layer is defined as the structure factor at 100% D_2O minus the structure factor at 8% D_2O. Consequently, the linear plot of D_2O/H_2O ratios versus the structure factors can obtain the structure factor phase signs for different diffraction orders. Detailed description of this method can be found elsewhere.[36, 38-39] The Fourier reconstruction of the scattering length density (SLD) profiles across the unit cell is calculated using the following equation:

$$\rho(x) = F_0 + 2\sum_{h=1}^{h_{max}} F_h \cos\left(\frac{2.\pi.h.x}{d}\right) \quad (6)$$

Here, x is the direction normal to the lipid bilayer membrane, x = 0 is the center for the unit cell. In this equation, F_0 is the SLD per volume of the sample, which puts the data on an absolute scale. The F_0 value for different lipid composition can be obtained by combining the

density and chemical composition of the model membrane.[40] As shown previously,[14, 41-42] the data can be adjusted by isotopic substitution (H/D) of certain parts of the lipid molecules. The known SLD difference between H and D sample can be linked with the area difference between the SLD profiles. The use of hydrogenated lipids and surfactants limits SLD changes, but it is sufficient for us to analyse the variation of SLDs in the unit cell.

2.6. Molecular dynamic (MD) simulation setup and simulation protocol

A model of the short periodicity phase (SPP) is simulated. Its composition structure is shown in Figure 1, containing N-lignoceroylsphingosine (CER), lignoceric acid (LA) and cholesterol (CHOL) with equimolar ratio of 1:1:1 in the bilayer structure. The surfactant (C_{16}HAB or IHAB) in the bilayer of CER, LA and CHOL is in the molar ratio of 1:2:2:2. This study provides useful insight into the hydration of SC lipids arranged in a bilayer structure that is perturbed by cationic surfactant to model the SPP using all-atom resolution while also combining the simulation model with neutron diffraction experiments. Molecular dynamics (MD) simulation is an increasingly promising technique for studying the SC, and numerous studies have already been performed.[43-47] These vary in resolution from coarse-grain to all-atom force fields, and SPP bilayers are more commonly studied than long periodicity phase (LPP) multilayers.[45]

Bilayer models with and without cationic surfactant were separately generated in rectangular boxes (X = Y ≠ Z) using CHARMM-GUI Membrane Builder.[48-50] Their initial box sizes were $4.5\times4.5\times10$ nm^3 and $5.1\times5.1\times10$ nm^3, respectively. All the MD simulations were run in the CHARMM36 (C36) force field, the C36 lipid force field was used with the TIP3P water model,[45, 51] force field parameters of surfactants were generated by CHARMM General Force Field (CGenFF) program.[52-53] 100 mM NaCl was used in these simulations.

All simulations including NVT, NPT ensemble and production MD were performed in

GROMACS 2016.3.[54-55] The temperature was initially maintained by the Berendsen thermostat with a time constant of 0.5 ps for initial equilibration; it was then changed to the Nosé−Hoover thermostat with the same time constant. Pressure was controlled at 1 bar using a Berendsen barostat for initial equilibration with a time constant of 0.5 ps and a compressibility of 4.5×10^{-5} bar^{-1}; in a subsequent production MD run, it was changed to a Parrinello−Rahman barostat with a time constant of 5 ps and a compressibility of 4.5×10^{-5} bar^{-1}. The semi-isotropic coupling (coupled separately in the xy and z direction) of the barostat was used to simulate a tensionless bilayer.

All of the bonds in lipid molecules were constrained using the LINCS algorithm36 while for water the SETTLE37 algorithm was used. A time step of 2 fs was used for simulations at 303 K, a cutoff of 1.2 nm was used for *van der Waals* and electrostatic interactions. Long-range electrostatic interaction was computed using the particle mesh Ewald (PME) method. The equilibration time for all of the systems was 500 ps (NVT), 1 ns (NPT) equilibration followed by 50 ns production MD. The final 5 ns run of MD simulation was used for calculation of equilibrium properties (production run). The configuration was sampled at every 0.5 ps in the production run. Visual Molecular Dynamics (VMD)[56] was used to create snapshots.

2.7. Simulation result analysis

Mass density profiles (MDPs) along the bilayer normal were calculated with a slab thickness of 0.2 Å. Radial distribution functions (RDFs) were calculated with the oxygen of CHOL, the head of CER, and the carboxyl carbon of LA to describe their hydration behavior and hydration change affected by surfactants.

3. RESULT AND DISCUSSION

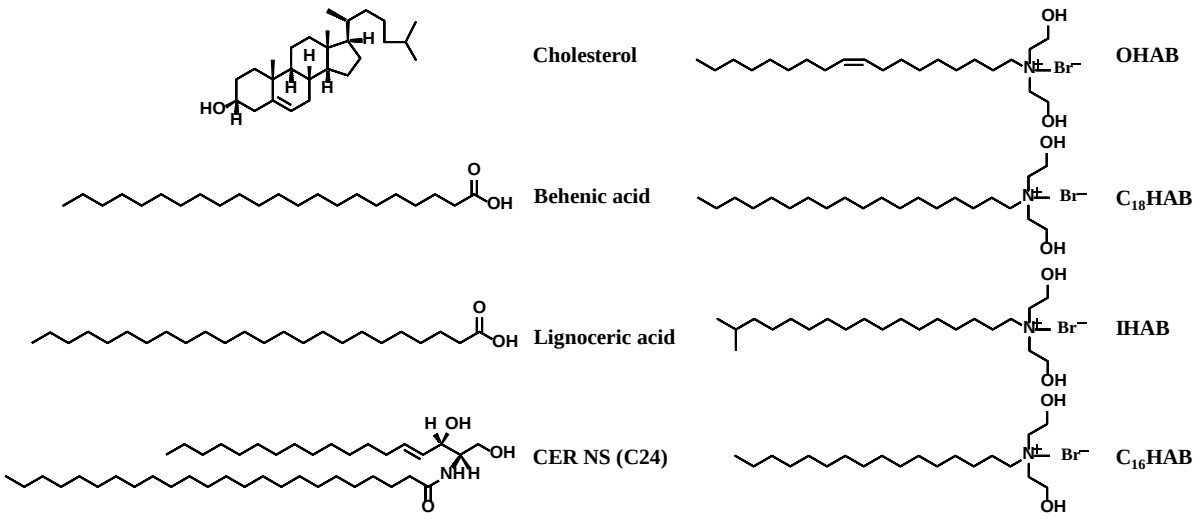

Figure 1. Structures of ceramide, cholesterol, fatty acids and surfactants.

Despite the superior amphiphilic properties of cationic surfactants, the toxicity limits their practical applications. One of the potential hazards of cationic surfactants as drug carrier and penetration enhancer is to cause skin irritancy such as redness and inflammation, which arise from the interactions between surfactants and skin lipids or proteins.[32-33, 57-58] Both the critical micellar concentration (CMC) and headgroup charge have been thought as the main impact factors.[59] Surfactants with high CMCs are more irritant than those with low CMCs, since surfactant monomers are thought to interact more strongly with SC proteins than the micelles. Additionally, ionic surfactants may exhibit stronger irritancy than nonionic surfactants because of the charge-driven electrostatic interactions with keratins in SC.

We have designed and synthesized four long-chain cationic surfactants with a large headgroup as shown in Figure 1, aiming to reduce the irritancy while keeping superior self-assembly capability. The long hydrophobic tail maintains the high hydrophobicity of surfactant with a low CMC. A large volume of surfactant headgroup weakens its binding to SC proteins through charge interaction. As the fluidity of surfactant's chain can also influence its performance as chemical enhancer in drug delivery,[1, 7, 30-31] the hydrophobic chain

architecture such as chain length, branching or unsaturation has been adjusted by increasing the chain length from C16 (C_{16}HAB) to C18 (C_{18}HAB), branched methyl group in isostearic alkyl chain (IHAB) and incorporation of one double bond in oleic chain (OHAB). This work aims to reveal the arrangements of these selected surfactants in model SC membranes and understand the impact of chain fluidity on the interactions between SC lipids and surfactants.

3.1. Critical micellar concentrations (CMCs)

Surface tension experiments were carried out to obtain the CMCs of the surfactants and the results are shown in Figure S1. Surface tension values drop with increasing surfactant concentration, and then they level off and become invariant beyond the CMC. The CMC values obtained from the surface tension curves (Table S2) decrease in the order of IHAB < C_{18}HAB < OHAB < C_{16}HAB.

Given the same headgroup of these surfactants, the variation of CMC can be explained by the chain architecture. For C_{16}HAB, OHAB and C_{18}HAB, the hydrocarbon chain length increases from C16 to C18. According to the Klevens equation,[60] the logarithm of CMC linearly decreases with increase in hydrophobic chain length of the surfactant, because of the increase of hydrophobicity with chain length. Thus, C_{16}HAB has the highest CMC value among all the surfactants. Comparing OHAB with C_{18}HAB, they both have the same number of hydrocarbon (C18) in the tail moiety. However, the cis-double bond configuration of oleic chain leads to a shorter equivalent chain length than that of straight chain, indicating a higher CMC for OHAB.

IHAB has the lowest CMC among all the surfactants. Normally, with the same number of carbons in the chain, the branched alkyl chain exhibits a better affinity with water than the straight one as it effectively shortens chain length,[61] resulting in a higher CMC for the branched surfactant. However, the influence of chain length is not well pronounced for IHAB because only one branched methyl group exists at the end of the alkyl tail. The major impact

of the branched methyl group is understood from how the alkyl chain of IHAB packs. The steric hindrance could well lead to more loose packing between the branched methyl groups. The surfactant could reach its saturation adsorption at a lower concentration than the straight-chain surfactants, resulting in the lower CMC of IHAB than that of C_{18}HAB.

3.2. Neutron diffraction pattern

Neutron diffraction measurements were performed to investigate the structures of CER/CHOL/FFA model membranes with and without surfactants. First, model SC lipid membrane without surfactant (CER^{Pure}) was studied. The composition for CER^{Pure} is presented in Table S1, consisting of an equimolar mixture of ceramide (CER NS (C24)), cholesterol and a fatty acid mixture (C22: C24 = 1: 1, molar ratio). The sample was hydrated and measured at 8% D_2O, 50% D_2O and 100% D_2O. Figure S2 shows the one-dimensional neutron diffraction profiles for CER^{Pure} at different contrasts. The sharp diffraction peaks suggest a highly oriented lamellar structure parallel to the silicon wafer substrate. From the diffraction patterns shown in Figure S2 a lamellar phase was observed together with the crystalline CHOL phase. The repeating distance (*d*) of the lamellar phase was calculated by the *q* value of each Bragg peak using Eq. 2, and the averaged *d* value was calculated by a least square fitting procedure, with the results with uncertainties listed in Table S1. The calculated periodicity of CER^{Pure} at 100% D_2O is 53.4 ± 0.6 Å, which is close to the reported repeating distance of the short periodicity phase (SPP).[12, 15] This value is also consistent with the SPP structure formed by the more complex CERs/CHOL/FFAs mixture containing ceramides from 5 CER subclasses and 7 fatty acids,[12, 15] displaying a more close mimicry of the human SC composition.[17, 24]

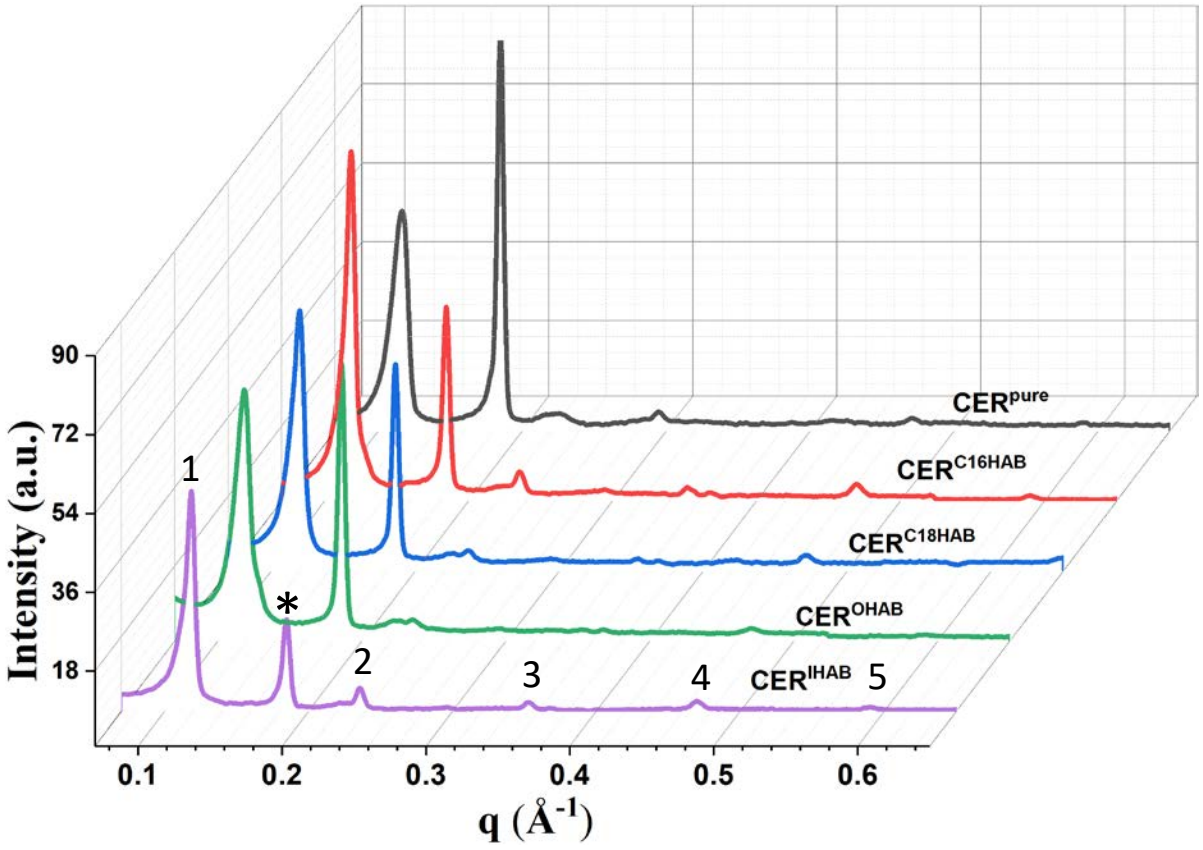

Figure 2. Neutron diffraction one dimensional plot of intensity vs *q* for the CER/CHOL/FFA membrane and the surfactant/CER/CHOL/FFA mixed membranes hydrated and measured at 100% D_2O, with each surfactant being controlled at 1mol%. The diffraction orders of the SPP lamellae are indicated by the numbers and the CHOL peaks by means of an asterisk. An enlarged graph is presented in Figure S3 to enable better viewing of the peaks from higher diffraction orders.

To investigate the interaction of surfactant with model SC membrane, a small amount of surfactant (1 mol% of total lipids) was added during membrane preparation. In total, four surfactant-SC lipids mixed membranes were investigated as shown in Table S1, i.e., CER^{C16HAB}, CER^{C18HAB}, CER^{IHAB} and CER^{OHAB}. Figure 2 shows the one-dimensional plot of scattering intensity *vs* scattering vector *q* for the surfactant/CER/CHOL/FFA mixed membranes hydrated and measured at 100% D_2O. The profile of CER^{Pure} is also presented for comparison. All one-dimensional curves have six diffraction orders from both the lamellar

structure of lipids and the crystalline CHOL phase. The numbers in Figure 2 indicate the five diffraction peaks from SPP, and the asterisk indicates the diffraction peak of phase separated CHOL (q = 0.19 Å^{-1}). No additional surfactant phase was observed, indicating that all the surfactants were incorporated into the SPP structure. The repeating distances of the SPP structure after adding surfactants were calculated to be 53.2 ± 0.3 Å, which is similar to that of 53.4 ± 0.5 Å for CER^{Pure}. Obviously, surfactants have very limited impact on the repeating distance of the lamellar structures, however, the Bragg peaks become more pronounced after adding surfactants as observed in Figure 2, especially for the higher order ones. This suggests that the lamellar structures become more ordered in the present of surfactants. Another notable difference between the 1D curves is the decrease of cholesterol peak intensity with the addition of surfactants, which will be discussed later in this paper.

Though little impact on the repeating distance of SPP is observed by adding surfactants, the arrangements of surfactants and the corresponding impacts they lead to the SPP unit cell are not clear yet. Therefore, the model membranes were hydrated and measured at 50% D_2O and 8% D_2O (Figure S4) to gain further structural information of the SPPs.

3.3. Structure factors and phase sign of SPP

The contrast variation method was used to determine the phase sign of the different diffraction orders.[36-37] In this case, neutron diffraction measurements were performed with all the model membranes at 8%, 50% and 100% D_2O in the mixed solvent of D_2O and H_2O. As shown in Figure S5, structure factors linearly change with the volume fraction of D_2O, indicating a centrosymmetric structure of the SPP unit cell with the phase sign of either +1 or −1. The choice of the unit cell origin fixes the h = 1 sign, it will be −1 if the origin is set at the bilayer center. The h = 2 sign is related to the water SLD profile, and it will be −1 when the water density profile is considered as positive.[62-63] The water structure factors can be derived by subtracting the structure factors at 8% D_2O from that at 100% D_2O. Assuming

water molecules locate at the unit cell boundary nearing the hydrophilic headgroup of lipids, the remaining phase signs are derived such that the obtained water SLD profile shows a maximum at ± d/2 and a relative flat distribution at the bilayer center. This gives a water phase sign of −, +, −, +, − for the five diffraction orders h = 1 ~ 5. Other phase sign combinations were tried as well but they give unrealistic water distributions. The amplitudes, phase signs and corresponding uncertainties of the structure factors are summarized in Table S3.

3.4. Neutron SLD profiles of model membranes and water distributions

The synthetic model SC membrane has a low hydration level of ~ 2 water molecules per lipid compared to phospholipid bilayers of ~ 12 to 35 molecules per lipid.[12, 38] It is speculated that the intermolecular hydrogen bonding between CER headgroups plays a significant role in providing barrier function to SC.[64-65] The low hydration level of the SC lipid matrix increases the hydrophobicity of the SC which contributes to the skin barrier function. However, the barrier function must be reduced to increase the permeability of SC for transdermal delivery systems. It is useful to understand the impact of surfactant on the hydration of model SC membranes.

The neutron SLD profiles were generated by Eq. 6 using the deduced phase signs and the corresponding structure factor amplitudes in Table S3. Figure 3A displays the SLD profiles of CER^{Pure} at 8% and 100% D_2O. As the positive neutron SLD for D_2O (6.35×10^{-6} Å^{-2}) and negative SLD for H_2O (-0.56×10^{-6} Å^{-2}) 8% D_2O leads to SLD = 0, making water effectively invisible to neutron at this contrast. The difference between the curves at 100% and 8% D_2O indicates the water SLD profile, which is presented as a solid line in Figure 3A. By this means, the water SLD profiles for the surfactant-CER mixed membranes were obtained and presented in Figure S6, and a comparison of the water profiles for the different membranes was made in Figure 3B.

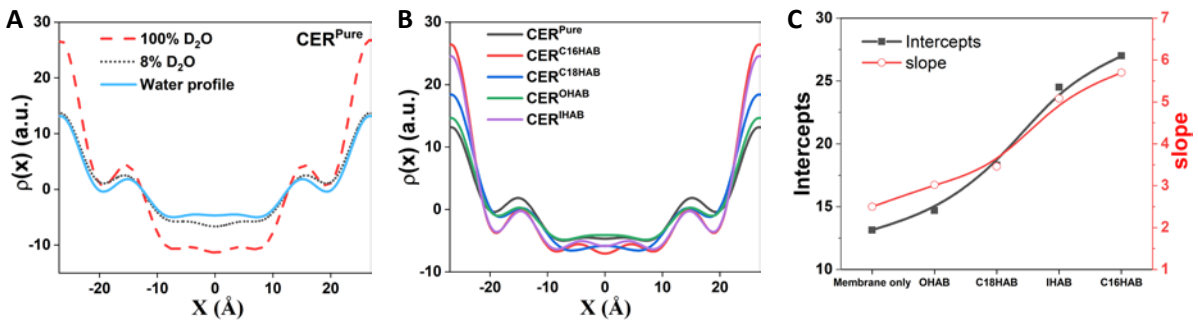

Figure 3. (A) The relative SLD profiles of CER^{Pure} hydrated and measured at 8% D_2O (black dotted line), and 100% D_2O (red dashed line). Difference profile between 8% and 100% D_2O shows the water SLD profile (blue solid line). (B) The relative water SLD profiles in different model membranes with each surfactant being controlled at 1 mol% of total lipids. (C) The intercepts and slopes calculated from the water SLD profiles in Figure 3B. The slope is an absolute value calculated from the SLD curve ranged from 20 Å ~ 27 Å.

For CER^{Pure}, the water SLD curve displays a maximum SLD at the boundary and a submaximal at −15 Å and +15 Å; meanwhile, a relative flat profile is observed in the central region. The maximum and submaximal water peaks indicate the locations of CER and FFA headgroups and the location of cholesterol headgroup, respectively. Because the water molecules prefer to bind to the polar hydrophilic moieties of lipid molecules, the relative flat SLD in the center suggests the location of alkyl tails. Therefore, lipid arrangements in the SPP unit cell can be estimated from the water SLD distribution. It is a typical SPP arrangement with the ceramide and fatty acid headgroups locate at the cell boundary and the hydrophobic tails interdigitate at the center of the cell. The cholesterol headgroup locates at the lipid/water interface with the tail extending to the bilayer center. This kind of lipid arrangement is consistent with the model proposed by Mojumdar et al.[15]

Surfactant significantly affects the hydration of the model SC membrane. A pronounced elevation of water SLD is observed at the cell boundary upon addition of surfactant as shown in Figure 3B, indicating the increase of the hydration level of the model membrane.

Meanwhile, the hydration level increases when more surfactant was added in Figure S7. The surfactant headgroup contains a cationic ammonium polar center and two hydroxyl groups, which is more attractive to water molecules than the neutral ceramide and fatty acid headgroup. Therefore, the increase of water SLD at the boundary region implies the location of surfactant headgroups. In addition, the submaximal SLD peaks at −15 Å and +15 Å decrease with surfactant addition. As discussed above, this water peak is attributed to the polar headgroup of cholesterol. The decrease of this peak indicates that the hydration level of cholesterol gets down in lipid-surfactant mixed membranes compared to CER^{Pure}. The polar headgroup of surfactant makes the boundary region effectively more competitive to bind with water during hydration process, which consequently results in the decease of cholesterol hydration level. This alteration also marks the change of structural packing over the headgroup region as a result of surfactant mixing.

Figure 3C compares the hydration level for different model membranes by calculating the intercepts and slopes of the water SLD profiles. Briefly, the intercepts are the SLD values at X = −27 Å and X = +27 Å in Figure 3B, and the slopes are calculated from the curves ranged from 20 Å < X < 27 Å. The intercept reflects the maximum increment of SLD in the presence of surfactant and the slope indicates the water density gradient in the hydrophilic part of the unit cell. Interestingly, both the intercepts and slopes in Figure 3C increase in the order of CER^{Pure} < CER^{OHAB} < CER^{C18HAB} < CER^{IHAB} < CER^{C16HAB}, suggesting the hydration gradient and water density at the unit cell boundaries increases in the same sequence. Considering the same headgroup and molar concentration of surfactants in the mixed model membrane, the difference points to the effect from the molecular architecture of surfactant tails, as shown in Figure 1. Obviously, C_{16}HAB is the most hydrophilic one due to the shortest C16 tail, thereby exhibiting the strongest binding ability with water. Comparing the branched IHAB with the straight-tail C_{18}HAB, the branched hydrocarbon chain exhibits a

better affinity with water than the straight one.[61] OHAB has the same number of hydrocarbon as C_{18}HAB, and theoretically the C=C double bond is more hydrophilic due to the higher electron density. However, the *cis*-configuration of the oleic chain may increase the steric effect in the hydrophobic chain region, making the equivalent molecular volume of OHAB tail larger than that of C_{18}HAB. OHAB molecules thus pack more loosely in the unit cell, and the corresponding density of water molecules is much lower than the others. Overall, the addition of surfactants increases the hydration level of the model SC membrane, but the exact extent of increase varies with the length and configuration of the hydrophobic chain.

3.5. Role of surfactant in the SPP unit cell

The structural role of surfactant in the SPP unit cell is investigated by comparing the SLD curves for different model membranes at 8% D_2O, where neutron scattering from water is negligible. Figure 4A depicts the SLD profiles for different model membranes hydrated and measured at 8% D_2O. It shows that the SLD level at the boundary increases extensively in the present of surfactant, consistent with presence of the surfactant headgroups in this region. Meanwhile, a reduction of SLD occurs in the central region between X = −18 Å and +18 Å, resulting from the overlapping of hydrogenated surfactant tails with the ceramide and fatty acid tails in the center of the SPP unit cell. Additionally, there is no interdigitation of surfactant tails as no distinct minimum of SLD can be observed at the zero position. This is reasonable as the maximum chain length of a fully extended surfactant tail is ~ 22 Å (C18), which is shorter than d/2 (~ 27 Å). Therefore, the possible arrangement of surfactant is that the headgroup locates at the unit cell boundary with the hydrophobic chain perpendicular to the basal plane.

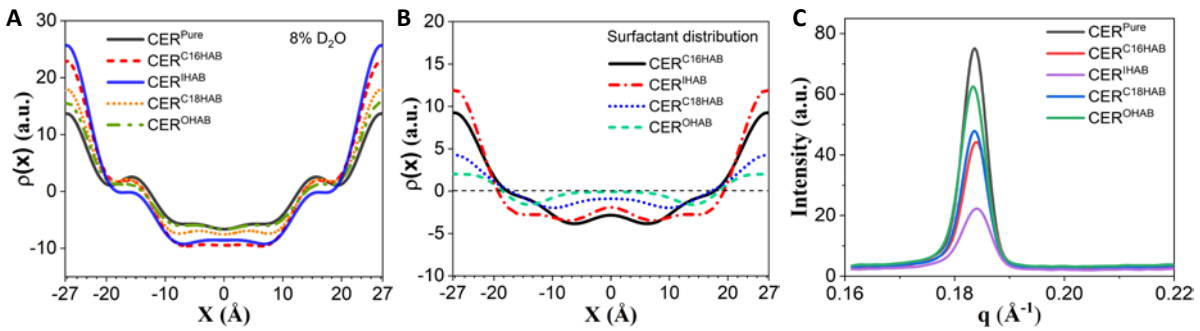

Figure 4. A) Relative SLD profiles for different model membranes hydrated at 8% D_2O; B) the difference plot between surfactant-lipid mixed membrane and pure lipid membrane at 8% D_2O indicates the surfactant SLD profile changes, C) Cholesterol peak intensity changes from different surfactant-lipid model membranes at 8% D_2O.

To further understand the impact of surfactant on the SPP unit cell, Figure 4B depicts the SLD profiles for the neat surfactants by subtracting the SLD profile for CER^{Pure} at 8% D_2O from those for lipid-surfactant mixed membranes at 8% D_2O. Though all the profiles exhibit an increased SLD value at the boundary when compared with CER^{Pure}, the increment of SLD varies between surfactants with increase in the order of $CER^{OHAB} < CER^{C18HAB} < CER^{C16HAB} < CER^{IHAB}$. Theoretically, the increment for all the model membranes should be identical due to the same headgroup and molar concentration of surfactants. It is most likely that the scattering intensity is not only from the surfactant. For the equimolar mixture of CER/CHOL/FFA, CHOL is partially incorporated into the lamellar structures and partially phase separated forming the crystalline phase.[15] Comparing the 1D diffraction patterns at 8% D_2O for all the model membranes, a significant variation of the CHOL peak intensity is observed in the presence of surfactant, and a detailed comparison of the peak alone within a narrow *q* range of 0.16 $Å^{-1}$ ~ 0.22 $Å^{-1}$ is made in Figure 4C. The intensity of the CHOL peak decreases in the order of $CER^{Pure} > CER^{OHAB} > CER^{C18HAB} > CER^{C16HAB} > CER^{IHAB}$, which is in a reversed order to the variation of the maximum SLD value at the boundary. It can be concluded that more CHOL molecules become incorporated into the SPP lamellae with

surfactant addition. These CHOL molecules lead to the increase of SLD in Figure 4B due to the higher SLD for the CHOL head (~ 0.49 × 10^{-6} $Å^{-2}$) than that of the surfactant head (~ 0.28 × 10^{-6} $Å^{-2}$). Meanwhile, the preference of CHOL binding with different surfactant can be demonstrated by the SLD change in the central region of the unit cell in Figure 4B. It shows that the minimum point of SLD shifts from the zero position to X = 5 ~ 10 Å, indicating that the CHOL tail is locating at this region as the interdigitation of protonated CHOL tail and surfactant tail results in a more negative SLD value. The SLD value at X = ~ ±8 Å decreases in the order of CER^{OHAB} > CER^{C18HAB} > CER^{C16HAB} > CER^{IHAB}, suggesting that the amount of CHOL binding with surfactant increases in the opposite order. This trend is consistent with the SLD changes at the headgroup region as discussed previously. Therefore, the SLD variations at the boundaries and in the central region together support the preferential CHOL binding with all the surfactants, resulting in its positional adjustment within the lipid bilayer.

Different interaction between surfactant and CHOL can be understood from the hydrophobic chain architecture of surfactants. First, OHAB with an oleic tail shows the weakest binding to cholesterol, evident from a minor increase of SLD at the boundary. This is because the CHOL molecule has lower affinity for unsaturated alkyl chains than for the saturated ones, consistent with the interpretation reported previously.[15, 66] IHAB shows the strongest binding to CHOL, consistent with the larger volume of the branched tail than the straight-chain one. It is reported that the interfacial area of CHOL is approximately twice of the straight hydrocarbon chain.[14-15] So one CHOL molecule can compensate two straight-chain surfactant molecules (C_{16}HAB and C_{18}HAB), but it can only compensate one branched surfactant (IHAB), indicating that the binding efficiency of IHAB to CHOL is much higher than other surfactants and supporting the largest SLD increase of IHAB as shown in Figure 4B. The SLD curves in Figure 4B suggest that CHOL has stronger binding with C_{16}HAB than

C_{18}HAB. The notable difference between them arises from the hydrophobic chain length, with shorter chain packing less densely and more favourable binding to CHOL.

3.6. Mechanism of surfactant-model SC interaction

MD simulations were performed with the selected surfactants of C_{16}HAB and IHAB to understand the hydration change of the model SC membrane upon surfactant mixing. Firstly, MD was performed with pure lipid membrane in Figure S8. Figure S8A depicts the chemical structures of lipid molecules and Figure S8B highlights the simulated outcome with the snapshot of the lamellar structure at 50 ns. Figure S8C shows a detailed analysis through inspection of mass density profiles (MDPs) of water, the headgroups and tails of the CER molecules. The thickness of the lamellae is calculated by the peak-to-peak distance of CER head being 5.25 nm, identical to the experimental results of 5.31 nm. The MDPs of the CER tail exhibits a 'W' shape in the middle region, consistent with the interdigitating arrangement of the CER molecules obtained from the neutron diffraction results. The Radial distribution functions (RDFs) for the hydration of the selected oxygen atoms and nitrogen atoms in the model membrane are presented in Figure S8D and S8E. The RDF profiles show primary peaks at ~ 2.4 Å, which is equal to the force range of H-bonding length. Notably, LA-H_2O RDFs show the highest peak intensity compared to CER-H_2O and CHOL-H_2O, indicating that the hydration of LA dominates the membrane hydration.

Upon introducing surfactants, the MD simulated molecular arrangements of the mixed surfactant-model SC membrane are shown in Figure 5 with Figure 5A and 5D for the membranes containing C16HAB (CER^{C16HAB}) and IHAB (CER^{IHAB}), respectively. For both CER^{C16HAB} and CER^{IHAB}, the snapshots of the membrane show that the overall bilayer arrangements are kept with surfactant mixing. The corresponding MDPs are shown in Figure 5B and 5E to depict the distributions and relative locations of the lipid, water and surfactant as a function of distance (*z* axis). The MDPs illustrate that the surfactant tails insert into the

bilayer with no interdigitation happening, and that the headgroups locate at the boundary of the bilayer. Comparing with the location of CER head, surfactant head extends more into the water layer by ~ 3.0 Å and ~ 1.2 Å for CER^{C16HAB} and CER^{IHAB}, respectively.

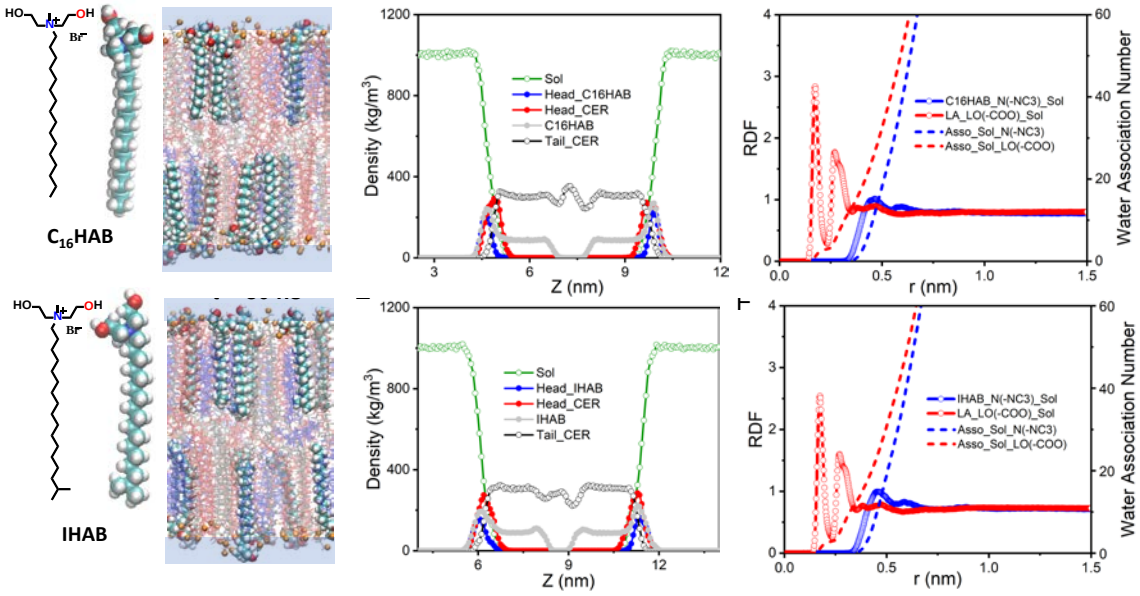

Figure 5. A) Chemical structures of $C_{16}HAB$, with RDF selection atoms shown in colours. Snapshot of the $C_{16}HAB$/CER/CHOL/FFA mixed membrane (CER^{C16HAB}) at the end of simulation. B) Mass density profiles of water, $C_{16}HAB$ and CER in CER^{C16HAB} as a function of distance. C) RDFs of selected atoms and corresponding water association number profiles. D) Chemical structures of IHAB, RDF selection atoms are shown in colours. Snapshot of the IHAB/CER/CHOL/FFA mixed membrane (CER^{IHAB}) at the end of simulation. E) Mass density profiles of water, IHAB and CER for CER^{IHAB} as a function of distance. F) RDFs of selected atoms and corresponding water association number profiles.

As discussed already with CER^{Pure}, the hydration of LA plays the key role in membrane hydration during simulation, the LA-H_2O RDFs for CER^{C16HAB} and CER^{IHAB} as shown in Figure 5C and 5F support this interpretation. Upon adding surfactant, both the primary and secondary peaks of LA-H_2O RDFs decrease in the order of CER^{Pure} > CER^{C16HAB} > CER^{IHAB}. The corresponding water association number of the first hydration layer decreases in the

order of 3.24 > 3.04 > 2.96 and the second hydration layer is in the order of 13.15 > 12.39 > 11.89 (Table S4). These results reveal the reduced hydration of LA by surfactants, associated with the strong electrostatic interaction between oppositely charged headgroups of surfactant and LA.[67-69] This can be proved by the RDFs of LA-C_{16}HAB and LA-IHAB in Figure S9, in which LA-IHAB has a stronger peak than that of LA-C_{16}HAB, indicating the stronger intermolecular association between the headgroups of IHAB and LA and weaker hydration of LA containing IHAB.

Furthermore, the hydration of surfactant headgroup (-HAB) was obtained by the RDFs of HAB-H_2O in Figure 5C and 5F. Although the extent of hydration of C_{16}HAB and IHAB headgroups is weaker than that of the negatively charged headgroup of LA, the water association numbers of C_{16}HAB and IHAB headgroups are much larger than that of LA-H_2O (Table S4). Thus, in spite of reduced hydration to anionic LA and some cationic surfactant molecules, the overall hydration level is enhanced as a result of adding surfactants into the membrane.

By combining the MD simulations with the experimental results, we schematically illustrate structural changes of the SC membrane before and after surfactant binding in Scheme 1. Scheme 1a depicts the lipid arrangements of CER^{Pure} in the SPP unit cell. In this model, the polar headgroups of CER, CHOL and FFAs locate at the unit cell boundaries with the hydrophobic chains projected perpendicular to the basal plane. Excess CHOL molecules form the phase separated CHOL phase. Scheme 1b presents the lipid arrangements after adding surfactants. The positively charged surfactant headgroups locate at the unit cell boundaries with their hydrophobic chains extending to the bilayer centre. The hydration of the boundary regions increases due to the strong hydration of surfactant headgroup. CHOL molecules follow similar style of structural alignment like surfactant but the mixing of

surfactant promoted the participation of more CHOL molecules and altered local packing, because the surfactant molecules create new binding sites for CHOL.

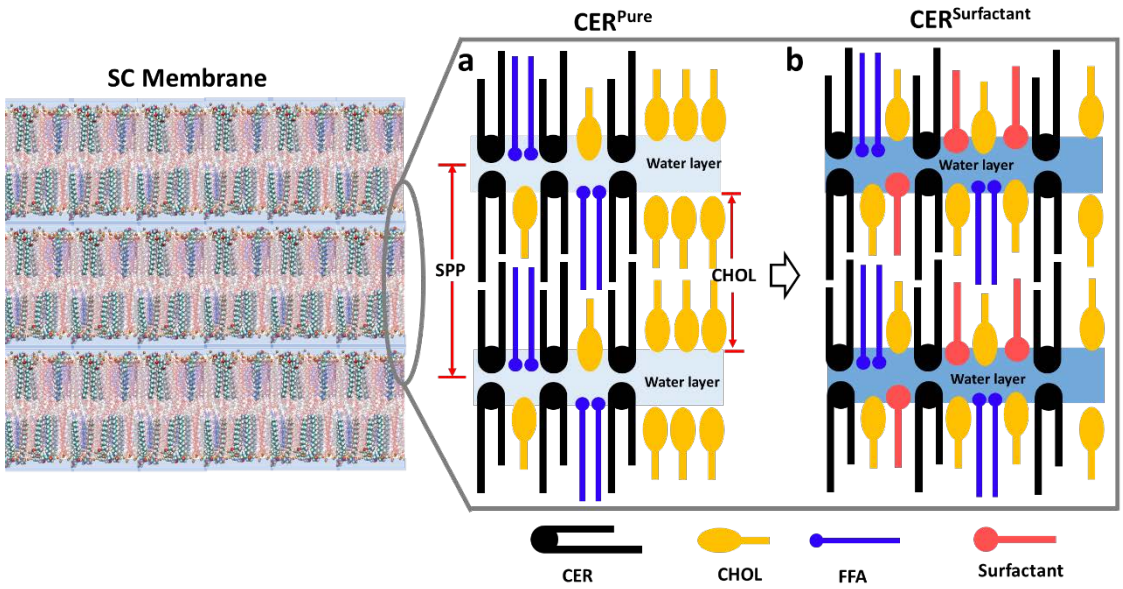

Scheme 1. Schematic for the bilayer structure of the SPP in model SC. (a) Pure SC membrane without surfactant, both the SPP phase and CHOL phase are presented with hydration layer in light blue. (b) Surfactant-lipid mixed model membrane, crystalline CHOL molecules migrate into the SPP with enhanced hydration of the bilayer (deep blue).

The above mechanism provides a new interpretation of surfactant as penetration enhancer in model SC. The surfactant plays a dual role in increasing the permeability of SC lipid membrane, which is different from the conventional penetration enhancer, i.e., ethanol, long-chain fatty acids and fatty alcohols.[70-73] On the one hand, more CHOL molecules incorporate into the SPP lamellae upon surfactant mixing, the decreased phase-separated CHOL level weakens the permeability of model SC.[74] On the other hand, hydrophilic surfactant headgroup remarkably increases the hydration level of model SC membrane and perturbs the lipid packing in the polar region, which improves the fluidity of fluid domain and consequently increases the permeability of the model SC membrane.[75]

4. CONCLUSIONS

A SC lipid model, consisting of a three simple component mixture of CER/CHOL/FFAs, produces the SPP structure that is highly similar to those reported from more complex lipid mixtures.[12, 15, 20] Neutron diffraction reveals that addition of surfactant significantly increases the overall hydration of the model membrane in the hydrophilic domain, and the hydration increases in the order of CER^{Pure} < CER^{OHAB} < CER^{C18HAB} < CER^{IHAB} < CER^{C16HAB}. The variation of hydration strongly depends on the hydrophilicity of the group of surfactant possessing the same headgroup but different chain architecture. The arrangement of surfactant in the SC membrane was examined from neutron SLD profiles and MD simulations. The results revealed a consistent picture of the projection of surfactant head-groups over the unit cell boundaries and tails extended to the center of the membrane bilayer. Interestingly, more CHOL molecules were incorporated into the SPP unit cell in the presence of surfactant, and the exact amount was affected by the molecular architecture of surfactant. Although incorporation of CHOL molecules affects the barrier function of the SC membrane, the more hydrophilic surfactant increases its hydration and fluidity and may eventually result in better permeability. Overall, this work has offered useful insight into the roles of surfactant and CHOL in mediating hydration and local structure of the SC membrane, providing important guidance for the development of surfactant-based transdermal drug delivery systems.

ACKNOWLEDGEMENTS

This work has received support from the European Union's Horizon 2020 research and innovation programme under the Marie Sklodowska-Curie Grant Agreement 665593 awarded to the Science and Technology Facilities Council. We would like to acknowledge the award of the neutron beam time on D16 at Institute Laue-Langevin, and the technical and scientific support. Thanks for the studentship support from the University of Manchester and China Scholarship Council (UoM-CSC joint PhD programme) to M.L. We also thank Dr. Shengjiang Yang (South China University of Technology) for his precious suggestion about simulation data analysis, and Dr. Gavin Stenning (ISIS) for the help with membrane characterization. An allocation time from the Shared Computation Facility (SCF) at the University of Manchester is gratefully acknowledged.

DECLARATION OF COMPETING INTERESTS

No competing financial interests.

AUTHOR CONTRIBUTIONS

Y Chen, PX Li and J R P Webster designed the project. Y Chen, PX Li, Z Wang, J Penfold and K Ma performed most of the experimental work. B Demé supported neutron diffraction experiments and data analysis. Y Chen and PX Li analyzed the data and prepared the overall manuscript. MR Liao performed the MD simulation work. All the authors contributed to manuscript writing and finalizing.

REFERENCES

(1) Prausnitz, M. R.; Langer, R. Transdermal drug delivery. *Nat. Biotechnol.* **2008,** *26* (11), 1261-1268.
(2) Wertz, P. W.; van den Bergh, B. The physical, chemical and functional properties of lipids in the skin and other biological barriers. *Chem. Phys. Lipids* **1998,** *91* (2), 85-96.
(3) Nemes, Z.; Steinert, P. M. Bricks and mortar of the epidermal barrier. *Exp. Mol. Med.* **1999,** *31* (1), 5-19.
(4) Barbero, A. M.; Frasch, H. F. Effect of stratum corneum heterogeneity, anisotropy, asymmetry and follicular pathway on transdermal penetration. *J. Controlled Release* **2017,** *260*, 234-246.
(5) Yu, B.; Langer, R.; Blankschtein, D.; Kim, K. H.; So, P. T. C. Visualization of Oleic Acid-induced Transdermal Diffusion Pathways Using Two-photon Fluorescence Microscopy. *J. Invest. Dermatol.* **2003,** *120* (3), 448-455.
(6) Johnson, M. E.; Blankschtein, D.; Langer, R. Evaluation of Solute Permeation through the Stratum Corneum: Lateral Bilayer Diffusion as the Primary Transport Mechanism. *J. Pharm. Sci.* **1997,** *86* (10), 1162-1172.
(7) Lawrence, M. J. Surfactant systems: their use in drug delivery. *Chem. Soc. Rev.* **1994,** *23* (6), 417-424.
(8) Karande, P.; Jain, A.; Mitragotri, S. Discovery of transdermal penetration enhancers by high-throughput screening. *Nat. Biotechnol.* **2004,** *22* (2), 192-197.
(9) Masukawa, Y.; Narita, H.; Shimizu, E.; Kondo, N.; Sugai, Y.; Oba, T.; Homma, R.; Ishikawa, J.; Takagi, Y.; Kitahara, T.; Takema, Y.; Kita, K. Characterization of overall ceramide species in human stratum corneum. *J. Lipid Res.* **2008,** *49* (7), 1466-1476.
(10) van Smeden, J.; Hoppel, L.; van der Heijden, R.; Hankemeier, T.; Vreeken, R. J.; Bouwstra, J. A. LC/MS analysis of stratum corneum lipids: ceramide profiling and discovery. *J. Lipid Res.* **2011,** *52* (6), 1211-1221.
(11) Bouwstra, J. A.; Cheng, K.; Gooris, G. S.; Weerheim, A.; Ponec, M. The role of ceramides 1 and 2 in the stratum corneum lipid organisation. *Biochim. Biophys. Acta* **1996,** *1300* (3), 177-186.
(12) Groen, D.; Gooris, G. S.; Barlow, D. J.; Lawrence, M. J.; van Mechelen, J. B.; Demé, B.; Bouwstra, J. A. Disposition of ceramide in model lipid membranes determined by neutron diffraction. *Biophys. J.* **2011,** *100* (6), 1481-1489.
(13) Mojumdar, E. H.; Gooris, G. S.; Barlow, D. J.; Lawrence, M. J.; Deme, B.; Bouwstra, J. A. Skin lipids: localization of ceramide and fatty acid in the unit cell of the long periodicity phase. *Biophys. J.* **2015,** *108* (11), 2670-2679.
(14) Mojumdar, E. H.; Gooris, G. S.; Groen, D.; Barlow, D. J.; Lawrence, M. J.; Demé, B.; Bouwstra, J. A. Stratum corneum lipid matrix: Location of acyl ceramide and cholesterol in the unit cell of the long periodicity phase. *Biochim. Biophys. Acta, Biomembr.* **2016,** *1858* (8), 1926-1934.
(15) Mojumdar, E. H.; Groen, D.; Gooris, G. S.; Barlow, D. J.; Lawrence, M. J.; Deme, B.; Bouwstra, J. A. Localization of Cholesterol and Fatty Acid in a Model Lipid Membrane: A Neutron Diffraction Approach. *Biophys. J.* **2013,** *105* (4), 911-918.
(16) Gooris, G. S.; Bouwstra, J. A. Infrared spectroscopic study of stratum corneum model membranes prepared from human ceramides, cholesterol, and fatty acids. *Biophys. J.* **2007,** *92* (8), 2785-2795.
(17) Gooris, G. S.; Kamran, M.; Kros, A.; Moore, D. J.; Bouwstra, J. A. Interactions of dipalmitoylphosphatidylcholine with ceramide-based mixtures. *Biochim. Biophys. Acta, Biomembr.* **2018,** *1860* (6), 1272-1281.
(18) Breathnach, A. S.; Goodman, T.; Stolinski, C.; Gross, M. Freeze-fracture replication of cells of stratum corneum of human epidermis. *J. Anat.* **1973,** *114* (Pt 1), 65-81.
(19) Bouwstra, J. A.; Gooris, G. S.; van der Spek, J. A.; Bras, W. Structural Investigations of Human Stratum Corneum by Small-Angle X-Ray Scattering. *J. Invest. Dermatol.* **1991,** *97* (6), 1005-1012.
(20) Bouwstra, J. A.; Gooris, G. S.; Dubbelaar, F. E. R.; Weerheim, A. M.; Ijzerman, A. P.; Ponec, M. Role of ceramide 1 in the molecular organization of the stratum corneum lipids. *J. Lipid Res.* **1998,** *39* (1), 186-196.
(21) Bouwstra, J.; Gooris, G.; Ponec, M. The lipid organisation of the skin barrier: liquid and crystalline domains coexist in lamellar phases. *J. Biol. Phys.* **2002,** *28* (2), 211-223.
(22) Wang, E.; Klauda, J. B. Structure and Permeability of Ceramide Bilayers and Multilayers. *J. Phys. Chem. B* **2019,** *123* (11), 2525-2535.
(23) Wang, E.; Klauda, J. B. Molecular Structure of the Long Periodicity Phase in the Stratum Corneum. *J. Am. Chem. Soc.* **2019,** *141* (42), 16930-16943.
(24) Wang, E.; Klauda, J. B. Simulations of Pure Ceramide and Ternary Lipid Mixtures as Simple Interior Stratum Corneum Models. *J. Phys. Chem. B* **2018,** *122* (10), 2757-2768.
(25) Moore, T. C.; Hartkamp, R.; Iacovella, C. R.; Bunge, A. L.; McCabe, C. Effect of Ceramide Tail Length on the Structure of Model Stratum Corneum Lipid Bilayers. *Biophys. J.* **2018,** *114* (1), 113-125.
(26) Hoopes, M. I.; Noro, M. G.; Longo, M. L.; Faller, R. Bilayer Structure and Lipid Dynamics in a Model Stratum Corneum with Oleic Acid. *J. Phys. Chem. B* **2011,** *115* (12), 3164-3171.

(27) Imokawa, G.; Akasaki, S.; Minematsu, Y.; Kawai, M. Importance of intercellular lipids in water-retention properties of the stratum corneum: induction and recovery study of surfactant dry skin. *Arch. Dermatol. Res.* **1989,** *281* (1), 45-51.
(28) Ananthapadmanabhan, K. P.; Mukherjee, S.; Chandar, P. Stratum corneum fatty acids: their critical role in preserving barrier integrity during cleansing. *Int. J. Cosmet. Sci.* **2013,** *35* (4), 337-345.
(29) Froebe, C. L.; Simion, F. A.; Rhein, L. D.; Cagan, R. H.; Kligman, A. Stratum corneum Lipid Removal by Surfactants: Relation to in vivo Irritation. *Dermatology* **1990,** *181* (4), 277-283.
(30) Som, I.; Bhatia, K.; Yasir, M. Status of surfactants as penetration enhancers in transdermal drug delivery. *J Pharm Bioallied Sci* **2012,** *4* (1), 2-9.
(31) Uchiyama, M.; Oguri, M.; Mojumdar, E. H.; Gooris, G. S.; Bouwstra, J. A. Free fatty acids chain length distribution affects the permeability of skin lipid model membranes. *Biochim. Biophys. Acta, Biomembr.* **2016,** *1858* (9), 2050-2059.
(32) Chen, Y.; Qiao, F.; Fan, Y.; Han, Y.; Wang, Y. Interactions of Cationic/Anionic Mixed Surfactant Aggregates with Phospholipid Vesicles and Their Skin Penetration Ability. *Langmuir* **2017,** *33* (11), 2760-2769.
(33) Chen, Y.; Ji, X.; Han, Y.; Wang, Y. Self-Assembly of Oleyl Bis(2-hydroxyethyl)methyl Ammonium Bromide with Sodium Dodecyl Sulfate and Their Interactions with Zein. *Langmuir* **2016,** *32* (32), 8212-8221.
(34) Chen, Y.; Qiao, F.; Fan, Y.; Han, Y.; Wang, Y. Interactions of Phospholipid Vesicles with Cationic and Anionic Oligomeric Surfactants. *J. Phys. Chem. B* **2017,** *121* (29), 7122-7132.
(35) Richard, D.; Ferrand, M.; Kearley, G. J. Analysis and Visualisation of Neutron-Scattering Data. *Journal of Neutron Research* **1996,** *4*, 33-39.
(36) Franks, N. P.; Lieb, W. R. The structure of lipid bilayers and the effects of general anaesthetics: An X-ray and neutron diffraction study. *J. Mol. Biol.* **1979,** *133* (4), 469-500.
(37) Zaccai, G.; Blasie, J. K.; Schoenborn, B. P. Neutron diffraction studies on the location of water in lecithin bilayer model membranes. *Proc. Natl. Acad. Sci. U. S. A.* **1975,** *72* (1), 376-380.
(38) Nagle, J. F.; Tristram-Nagle, S. Structure of lipid bilayers. *Biochimica et Biophysica Acta (BBA) - Reviews on Biomembranes* **2000,** *1469* (3), 159-195.
(39) Worcester, D. L.; Franks, N. P. Structural analysis of hydrated egg lecithin and cholesterol bilayers II. Neutron diffraction. *J. Mol. Biol.* **1976,** *100* (3), 359-378.
(40) Harroun, T. A.; Katsaras, J.; Wassall, S. R. Cholesterol Hydroxyl Group Is Found To Reside in the Center of a Polyunsaturated Lipid Membrane. *Biochemistry* **2006,** *45* (4), 1227-1233.
(41) Wiener, M. C.; White, S. H. Fluid bilayer structure determination by the combined use of x-ray and neutron diffraction. II. "Composition-space" refinement method. *Biophys. J.* **1991,** *59* (1), 174-185.
(42) Wiener, M. C.; King, G. I.; White, S. H. Structure of a fluid dioleoylphosphatidylcholine bilayer determined by joint refinement of x-ray and neutron diffraction data. I. Scaling of neutron data and the distributions of double bonds and water. *Biophys. J.* **1991,** *60* (3), 568-576.
(43) Das, C.; Noro, M. G.; Olmsted, P. D. Lamellar and Inverse Micellar Structures of Skin Lipids: Effect of Templating. *Phys. Rev. Lett.* **2013,** *111* (14), 148101.
(44) Gupta, R.; Rai, B. Molecular Dynamics Simulation Study of Skin Lipids: Effects of the Molar Ratio of Individual Components over a Wide Temperature Range. *J. Phys. Chem. B* **2015,** *119* (35), 11643-11655.
(45) Klauda, J. B.; Venable, R. M.; Freites, J. A.; O'Connor, J. W.; Tobias, D. J.; Mondragon-Ramirez, C.; Vorobyov, I.; MacKerell, A. D.; Pastor, R. W. Update of the CHARMM All-Atom Additive Force Field for Lipids: Validation on Six Lipid Types. *J. Phys. Chem. B* **2010,** *114* (23), 7830-7843.
(46) Wang, E.; Klauda, J. B. Molecular Dynamics Simulations of Ceramide and Ceramide-Phosphatidylcholine Bilayers. *J. Phys. Chem. B* **2017,** *121* (43), 10091-10104.
(47) Wang, E.; Klauda, J. B. Models for the Stratum Corneum Lipid Matrix: Effects of Ceramide Concentration, Ceramide Hydroxylation, and Free Fatty Acid Protonation. *J. Phys. Chem. B* **2018,** *122* (50), 11996-12008.
(48) Jo, S.; Kim, T.; Im, W. Automated Builder and Database of Protein/Membrane Complexes for Molecular Dynamics Simulations. *PLoS ONE* **2007,** *2* (9), e880.
(49) Lee, J.; Cheng, X.; Swails, J. M.; Yeom, M. S.; Eastman, P. K.; Lemkul, J. A.; Wei, S.; Buckner, J.; Jeong, J. C.; Qi, Y.; Jo, S.; Pande, V. S.; Case, D. A.; Brooks, C. L.; MacKerell, A. D.; Klauda, J. B.; Im, W. CHARMM-GUI Input Generator for NAMD, GROMACS, AMBER, OpenMM, and CHARMM/OpenMM Simulations Using the CHARMM36 Additive Force Field. *J. Chem. Theory Comput.* **2016,** *12* (1), 405-413.
(50) Wu, E. L.; Cheng, X.; Jo, S.; Rui, H.; Song, K. C.; Dávila-Contreras, E. M.; Qi, Y.; Lee, J.; Monje-Galvan, V.; Venable, R. M.; Klauda, J. B.; Im, W. CHARMM-GUI Membrane Builder toward realistic biological membrane simulations. *J. Comput. Chem.* **2014,** *35* (27), 1997-2004.
(51) Durell, S. R.; Brooks, B. R.; Ben-Naim, A. Solvent-Induced Forces between Two Hydrophilic Groups. *J. Phys. Chem.* **1994,** *98* (8), 2198-2202.
(52) Vanommeslaeghe, K.; Hatcher, E.; Acharya, C.; Kundu, S.; Zhong, S.; Shim, J.; Darian, E.; Guvench, O.; Lopes, P.; Vorobyov, I.; Mackerell Jr., A. D. CHARMM general force field: A force field for drug-like molecules compatible with the CHARMM all-atom additive biological force fields. *J. Comput. Chem.* **2010,** *31* (4), 671-

690.
(53) Yu, W.; He, X.; Vanommeslaeghe, K.; MacKerell Jr., A. D. Extension of the CHARMM general force field to sulfonyl-containing compounds and its utility in biomolecular simulations. *J. Comput. Chem.* **2012,** *33* (31), 2451-2468.
(54) Hess, B.; Kutzner, C.; van der Spoel, D.; Lindahl, E. GROMACS 4: Algorithms for Highly Efficient, Load-Balanced, and Scalable Molecular Simulation. *J. Chem. Theory Comput.* **2008,** *4* (3), 435-447.
(55) Pronk, S.; Páll, S.; Schulz, R.; Larsson, P.; Bjelkmar, P.; Apostolov, R.; Shirts, M. R.; Smith, J. C.; Kasson, P. M.; van der Spoel, D.; Hess, B.; Lindahl, E. GROMACS 4.5: a high-throughput and highly parallel open source molecular simulation toolkit. *Bioinformatics* **2013,** *29* (7), 845-854.
(56) Humphrey, W.; Dalke, A.; Schulten, K. VMD: Visual molecular dynamics. *J. Mol. Graph.* **1996,** *14* (1), 33-38.
(57) Zhou, C.; Wang, D.; Cao, M.; Chen, Y.; Liu, Z.; Wu, C.; Xu, H.; Wang, S.; Wang, Y. Self-Aggregation, Antibacterial Activity, and Mildness of Cyclodextrin/Cationic Trimeric Surfactant Complexes. *ACS Appl. Mater. Interfaces* **2016,** *8* (45), 30811-30823.
(58) Effendy, I.; Maibach, H. I. Surfactants and experimental irritant contact dermatitis. *Contact Dermatitis* **1995,** *33* (4), 217-25.
(59) Lemerya, E.; Briancon, S.; Chevalier, Y.; Bordes, C.; Oddos, T.; Gohier, A.; Bolzinger, M. A. Skin toxicity of surfactants: Structure/toxicity relationships. *Colloids Surf., A* **2015,** *469*, 166-179.
(60) Klevens, H. B. Structure and aggregation in dilate solution of surface active agents. *J. Am. Oil Chem. Soc.* **1953,** *30* (2), 74-80.
(61) Sagisaka, M.; Narumi, T.; Niwase, M.; Narita, S.; Ohata, A.; James, C.; Yoshizawa, A.; Taffin de Givenchy, E.; Guittard, F.; Alexander, S.; Eastoe, J. Hyperbranched Hydrocarbon Surfactants Give Fluorocarbon-like Low Surface Energies. *Langmuir* **2014,** *30* (21), 6057-6063.
(62) Pebay-Peyroula, E.; Dufourc, E. J.; Szabo, A. G. Location of diphenyl-hexatriene and trimethylammonium-diphenyl-hexatriene in dipalmitoylphosphatidylcholine bilayers by neutron diffraction. *Biophys. Chem.* **1994,** *53* (1), 45-56.
(63) Léonard, A.; Escrive, C.; Laguerre, M.; Pebay-Peyroula, E.; Néri, W.; Pott, T.; Katsaras, J.; Dufourc, E. J. Location of Cholesterol in DMPC Membranes. A Comparative Study by Neutron Diffraction and Molecular Mechanics Simulation. *Langmuir* **2001,** *17* (6), 2019-2030.
(64) Moore, D. J.; Rerek, M. E.; Mendelsohn, R. Role of Ceramides 2 and 5 in the Structure of the Stratum Corneum Lipid Barrier. *Int. J. Cosmet. Sci.* **1999,** *21* (5), 353-368.
(65) Moore, D. J.; Rerek, M. E. Insights into the molecular organization of lipids in the skin barrier from infrared spectroscopy studies of stratum corneum lipid models. *Acta Derm. Venereol. Suppl. (Stockh.)* **2000,** *208*, 16-22.
(66) Kučerka, N.; Marquardt, D.; Harroun, T. A.; Nieh, M.-P.; Wassall, S. R.; Katsaras, J. The Functional Significance of Lipid Diversity: Orientation of Cholesterol in Bilayers Is Determined by Lipid Species. *J. Am. Chem. Soc.* **2009,** *131* (45), 16358-16359.
(67) Chen, Z.; Liao, M.; Zhang, L.; Zhou, J. Molecular simulations on the hydration and underwater oleophobicity of zwitterionic self-assembled monolayers. *AIChE J.* **2021,** *67* (2), e17103.
(68) Cheng, G.; Liao, M.; Zhao, D.; Zhou, J. Molecular Understanding on the Underwater Oleophobicity of Self-Assembled Monolayers: Zwitterionic versus Nonionic. *Langmuir* **2017,** *33* (7), 1732-1741.
(69) Liao, M.; Cheng, G.; Zhou, J. Underwater Superoleophobicity of Pseudozwitterionic SAMs: Effects of Chain Length and Ionic Strength. *J. Phys. Chem. C* **2017,** *121* (32), 17390-17401.
(70) Aungst, B. J. Structure/Effect Studies of Fatty Acid Isomers as Skin Penetration Enhancers and Skin Irritants. *Pharm. Res.* **1989,** *6* (3), 244-247.
(71) Aungst, B. J.; J. Rogers, N.; Shefter, E. Enhancement of naloxone penetration through human skin in vitro using fatty acids, fatty alcohols, surfactants, sulfoxides and amides. *Int. J. Pharm.* **1986,** *33* (1), 225-234.
(72) Bommannan, D.; Potts, R. O.; Guy, R. H. Examination of the effect of ethanol on human stratum corneum in vivo using infrared spectroscopy. *J. Controlled Release* **1991,** *16* (3), 299-304.
(73) Krill, S. L.; Knutson, K.; Higuchi, W. I. Ethanol effects on the stratum corneum lipid phase behavior. *Biochim. Biophys. Acta, Biomembr.* **1992,** *1112* (2), 273-280.
(74) Sochorová, M.; Audrlická, P.; Červená, M.; Kováčik, A.; Kopečná, M.; Opálka, L.; Pullmannová, P.; Vávrová, K. Permeability and microstructure of cholesterol-depleted skin lipid membranes and human stratum corneum. *J. Colloid Interface Sci.* **2019,** *535*, 227-238.
(75) Marjukka Suhonen, T.; Bouwstra, J. A.; Urtti, A. Chemical enhancement of percutaneous absorption in relation to stratum corneum structural alterations. *J. Control. Release* **1999,** *59* (2), 149-161.

SUPPORTING INFORMATION

Table S1. Lipid composition, the component molar ratios and the repeating distance for different model membranes at different D_2O volume fractions.

Membrane Name	Lipid composition	Molar ratio	Repeat distance (Å)	D_2O (%)
CER^{pure}	CER/CHOL/FFA	1:1:1	53.3 ± 0.3	8
			53.3 ± 0.3	50
			53.4 ± 0.6	100
CER^{C16HAB}	CER/CHOL/FFA/C_{16}HAB	1:1:1:0.03	53.2 ± 0.2	8
			53.2 ± 0.2	50
			53.2 ± 0.3	100
CER^{C18HAB}	CER/CHOL/FFA/C_{18}HAB	1:1:1:0.03	52.9 ± 0.4	8
			53.2 ± 0.2	50
			53.1 ± 0.3	100
CER^{OHAB}	CER/CHOL/FFA/OHAB	1:1:1:0.03	53.0 ± 0.3	8
			53.1 ± 0.2	50
			53.3 ± 0.2	100
CER^{IHAB}	CER/CHOL/FFA/IHAB	1:1:1:0.03	53.2 ± 0.2	8
			53.2 ± 0.3	50
			53.2 ± 0.3	100
CER^{OHAB-2}	CER/CHOL/FFA/OHAB	1:1:1:0.06	53.3 ± 0.2	8
			53.1 ± 0.3	50
			53.2 ± 0.3	100

Table S2. The scattering length density (SLD) and CMC values for surfactants and cholesterol (CHOL).

Surfactant	SLD head ($\times 10^{-6}$ Å^{-2})	SLD tail ($\times 10^{-6}$ Å^{-2})	CMC (mM)
C_{16}HAB	0.28	-0.36	0.85
OHAB	0.28	-0.36	0.52
C_{18}HAB	0.28	-0.34	0.23
IHAB	0.28	-0.35	0.12
CHOL	0.49	-0.50	–

Cetyl bis(2-hydroxyethyl)-methylammonium bromide C_{16}HAB, oleyl bis(2-hydroxyethyl)-methylammonium bromide OHAB, stearyl bis(2-hydroxyethyl)-methylammonium bromide C_{18}HAB, and isostearyl bis(2-hydroxyethyl)-methylammonium bromide IHAB.

Table S3. The structure factors with their corresponding phase signs and standard errors for all the model SC membranes.

Membrane type	D_2O (%)	F1	F2	F3	F4	F5
CER^{pure}	8	-3.98 ± 0.07	0.89 ± 0.07	-0.57 ± 0.19	1.16 ± 0.06	-0.73 ± 0.12
	50	-5.45 ± 0.02	0.99 ± 0.05	-0.89 ± 0.12	1.91 ± 0.04	-0.97 ± 0.05
	100	-6.87 ± 0.07	1.49 ± 0.06	-1.26 ± 0.10	2.40 ± 0.05	-1.41 ± 0.05
CER^{C16HAB}	8	-6.30 ± 0.07	1.75 ± 0.06	-1.02 ± 0.09	1.61 ± 0.05	-0.78 ± 0.07
	50	-8.88 ± 0.06	3.13 ± 0.05	-2.18 ± 0.04	2.88 ± 0.03	-1.41 ± 0.04
	100	-11.04 ± 0.05	4.37 ± 0.04	-3.21 ± 0.03	3.83 ± 0.02	-2.15 ± 0.03
CER^{C18HAB}	8	-4.92 ± 0.07	1.40 ± 0.08	-0.64 ± 0.13	1.20 ± 0.05	-0.81 ± 0.09
	50	-7.16 ± 0.06	2.09 ± 0.05	-1.33 ± 0.06	2.05 ± 0.04	-1.05 ± 0.05
	100	-9.15 ± 0.04	3.00 ± 0.04	-2.00 ± 0.04	2.74 ± 0.02	-1.28 ± 0.03
CER^{OHAB}	8	-4.24 ± 0.06	1.28 ± 0.07	-0.72 ± 0.11	0.96 ± 0.07	-0.64 ± 0.08
	50	-5.54 ± 0.04	1.85 ± 0.04	-1.03 ± 0.07	1.63 ± 0.03	-0.77 ± 0.04
	100	-7.41 ± 0.04	2.66 ± 0.04	-1.70 ± 0.04	2.21 ± 0.02	-1.18 ± 0.03
CER^{IHAB}	8	-6.35 ± 0.07	2.60 ± 0.06	-1.47 ± 0.07	1.68 ± 0.05	-0.74 ± 0.19
	50	-8.23 ± 0.06	3.66 ± 0.04	-2.37 ± 0.04	2.56 ± 0.03	-1.22 ± 0.04
	100	-10.75 ± 0.04	5.18 ± 0.03	-3.47 ± 0.02	3.77 ± 0.02	-1.94 ± 0.02
CER^{OHAB-2}	8	-4.91 ± 0.05	1.70 ± 0.06	-1.10 ± 0.06	1.22 ± 0.04	-0.77 ± 0.03
	50	-6.59 ± 0.04	2.57 ± 0.07	-1.52 ± 0.05	2.13 ± 0.02	-1.25 ± 0.02
	100	-8.87 ± 0.04	3.63 ± 0.06	-2.60 ± 0.03	3.22 ± 0.03	-1.67 ± 0.04

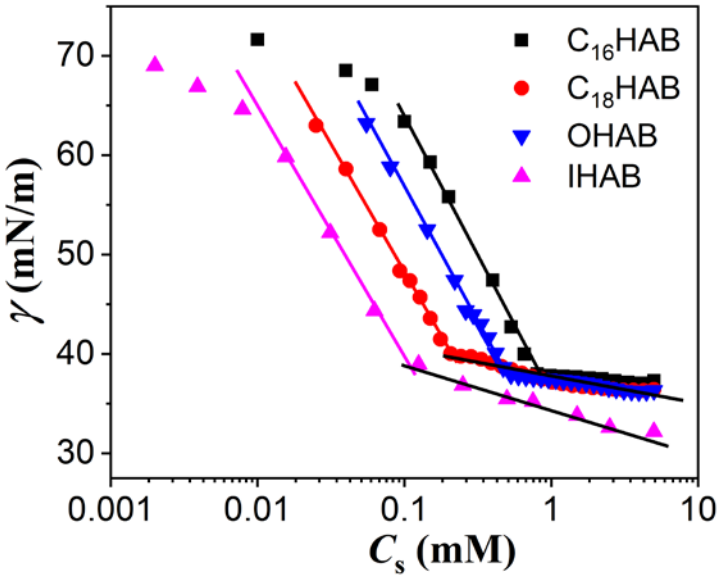

Figure S1. Surface tension curves for surfactants plotted against C_s, where C_s is surfactant concentration in mM.

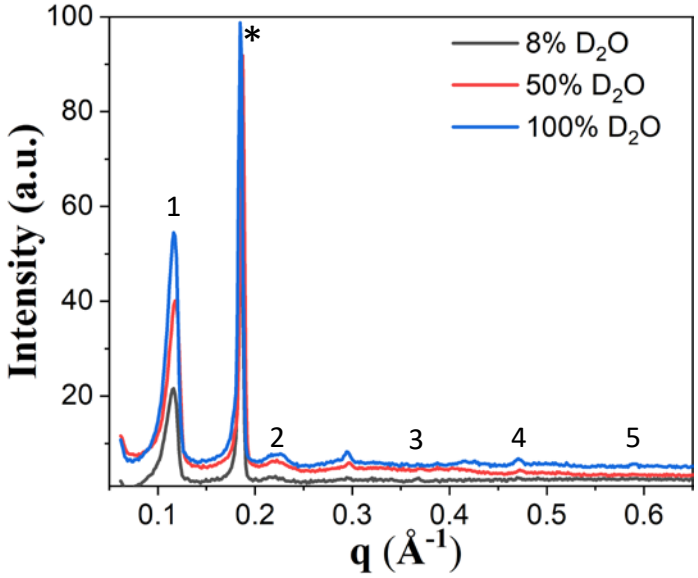

Figure S2. Neutron diffraction one-dimensional plots of intensity vs *q* for CER^{pure} hydrated and measured at 8%, 50% and 100% D_2O. The SPP diffraction orders are marked by numbers and the CHOL peak by using asterisks.

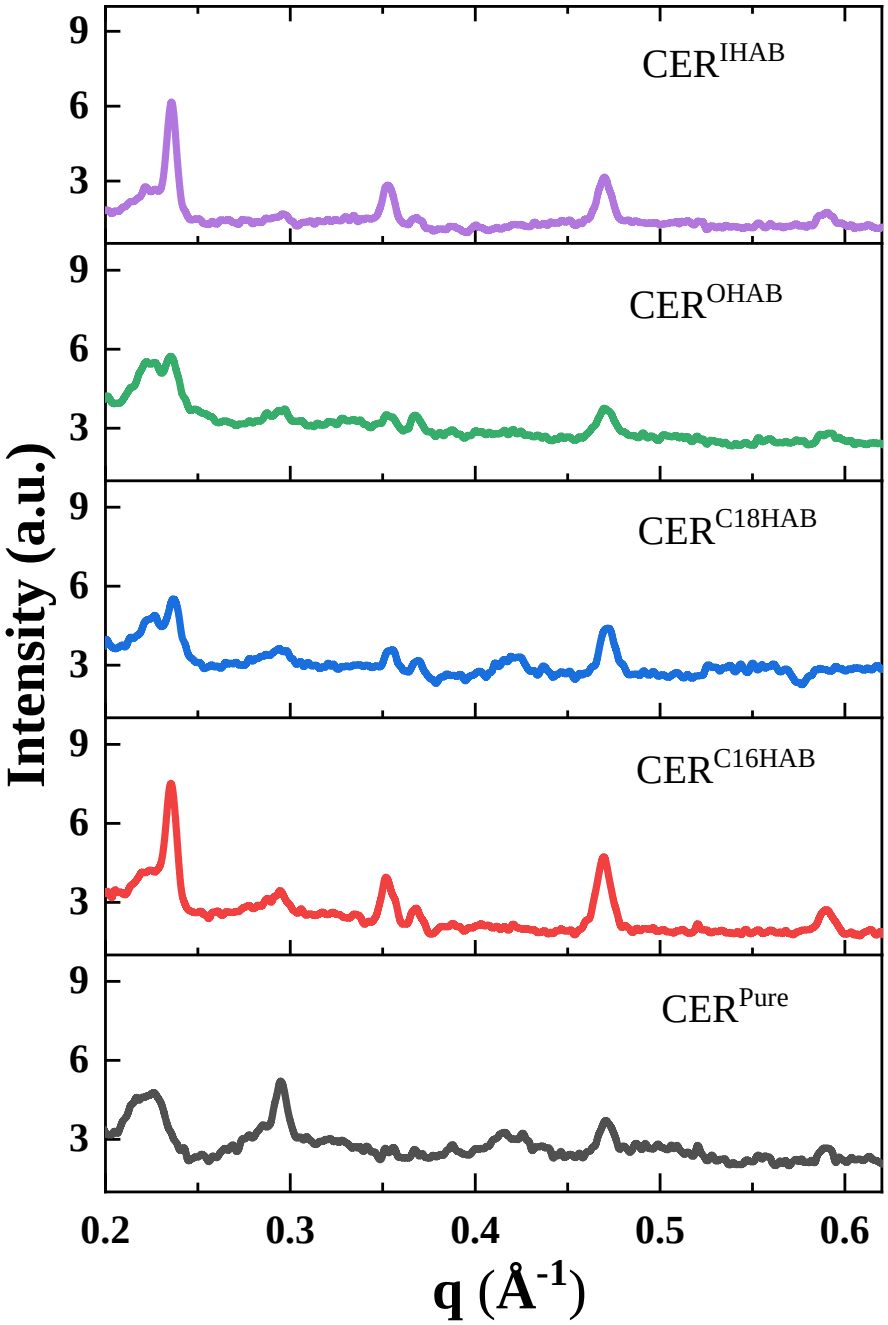

Figure S3. Neutron diffraction one dimensional plot of intensity vs *q* for the pure membrane and the surfactant/SC mixed membranes hydrated and measured at 100% D_2O, with each surfactant being controlled at 1mol%. The *q* range is narrow to show the 2^{nd}-5^{th} diffraction orders clearly in Figure 2.

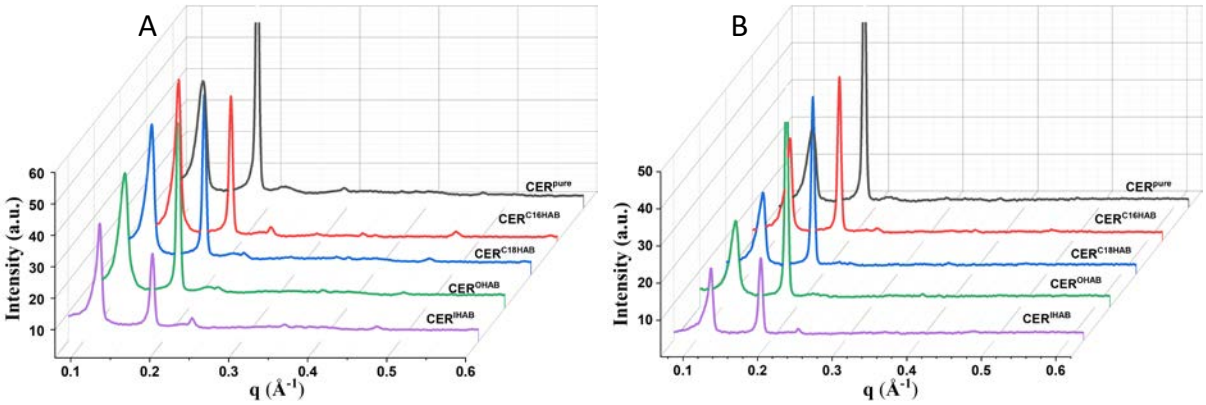

Figure S4. Neutron diffraction one-dimensional plots of intensity vs *q* for different model membranes hydrated and measured at A) 50% D_2O, B) 8% D_2O.

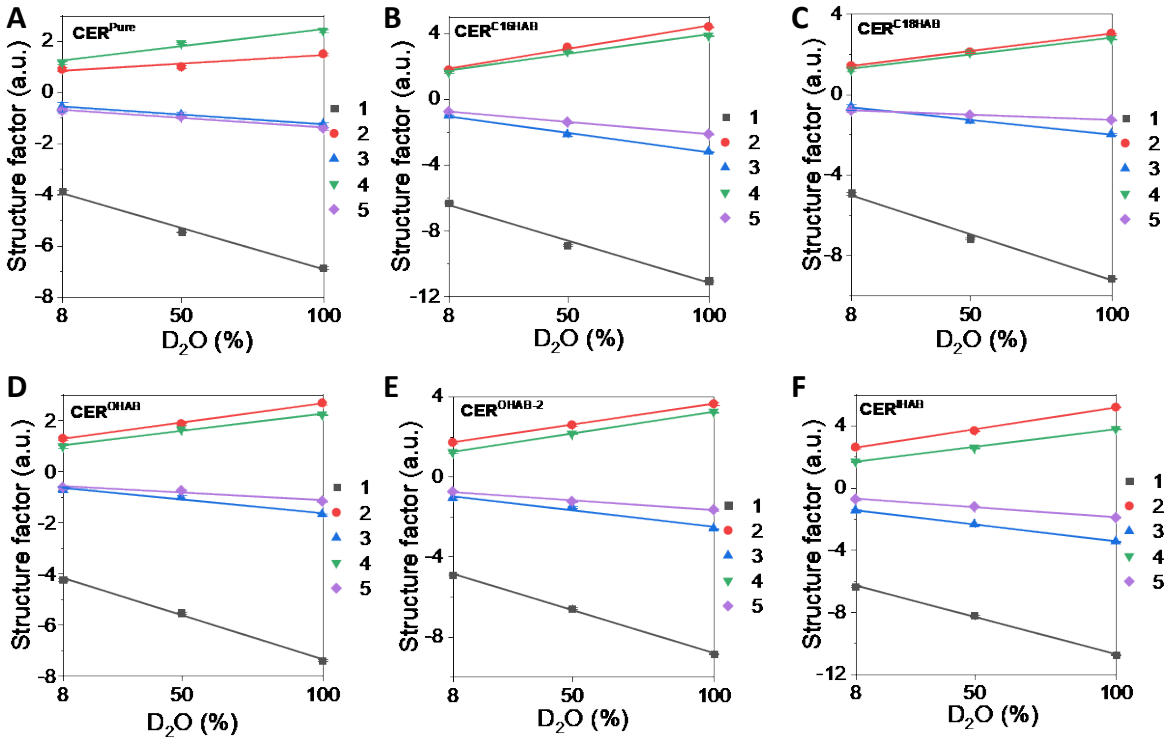

Figure S5. Relative structure factors of the five diffraction orders for mode membranes as a function of D_2O/H_2O volume ratio: A) CER^{pure}, B) CER^{C16HAB}, C) CER^{C18HAB}, D) CER^{OHAB}, E) CER^{OHAB-2}, F) CER^{IHAB}. The numbers given in the plots indicate the different diffraction orders.

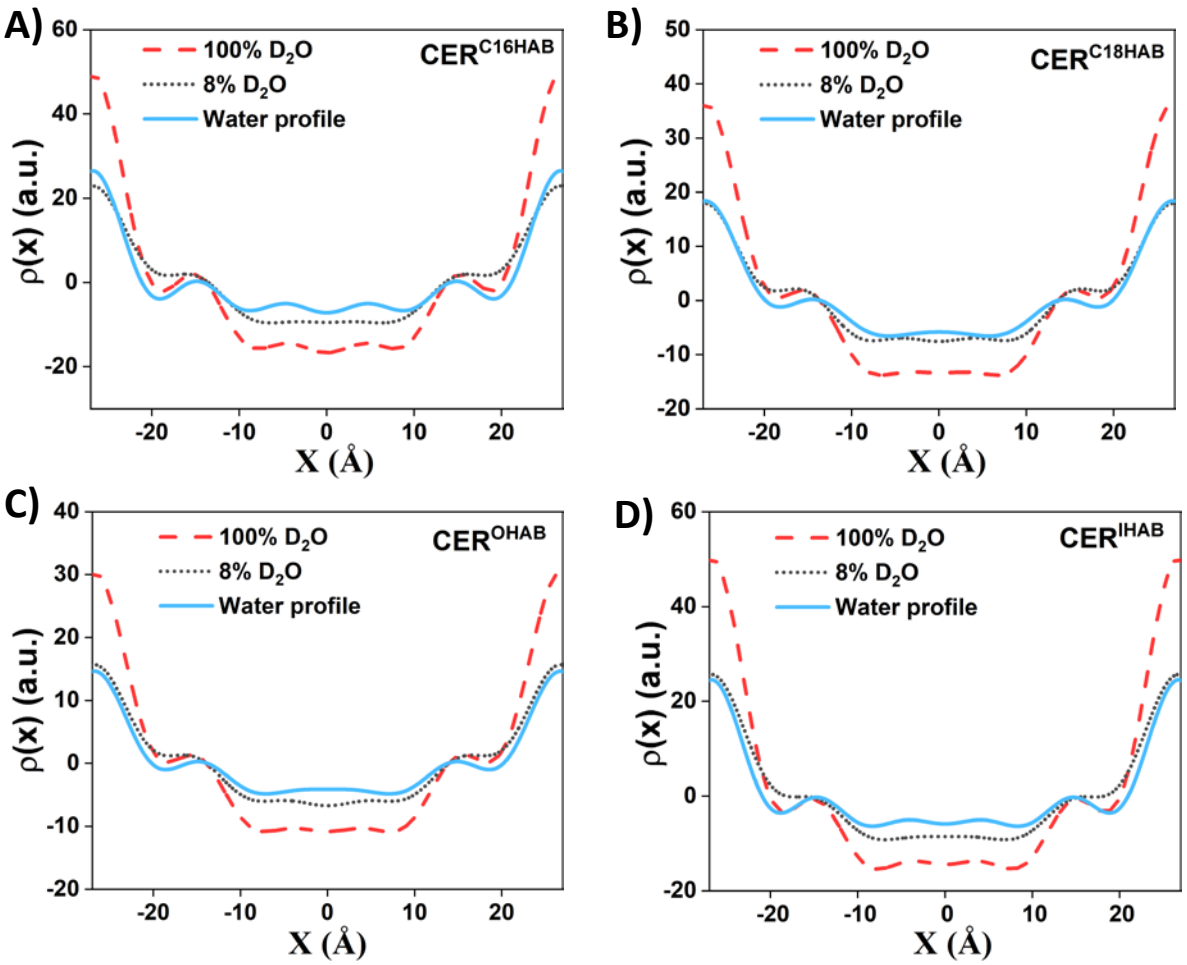

Figure S6. The relative SLD profiles of the CER/CHOL/FFA/surfactant mixed membranes hydrated and measured at 8% D_2O (black dotted line), 100% D_2O (red dashed line). The difference between 8% and 100% D_2O shows the water SLD profile (blue solid line). A) CER^{C16HAB}, B) CER^{C18HAB}, C) CER^{OHAB} and D) CER^{IHAB}.

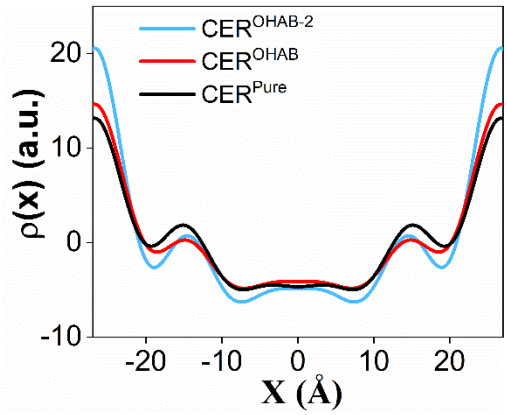

Figure S7. Water SLD profiles for CER^{Pure}, CER^{OHAB} (OHAB concentration at 1% molar ratio of total lipids) and CER^{OHAB-2} (OHAB concentration at 2% molar ratio of total lipids).

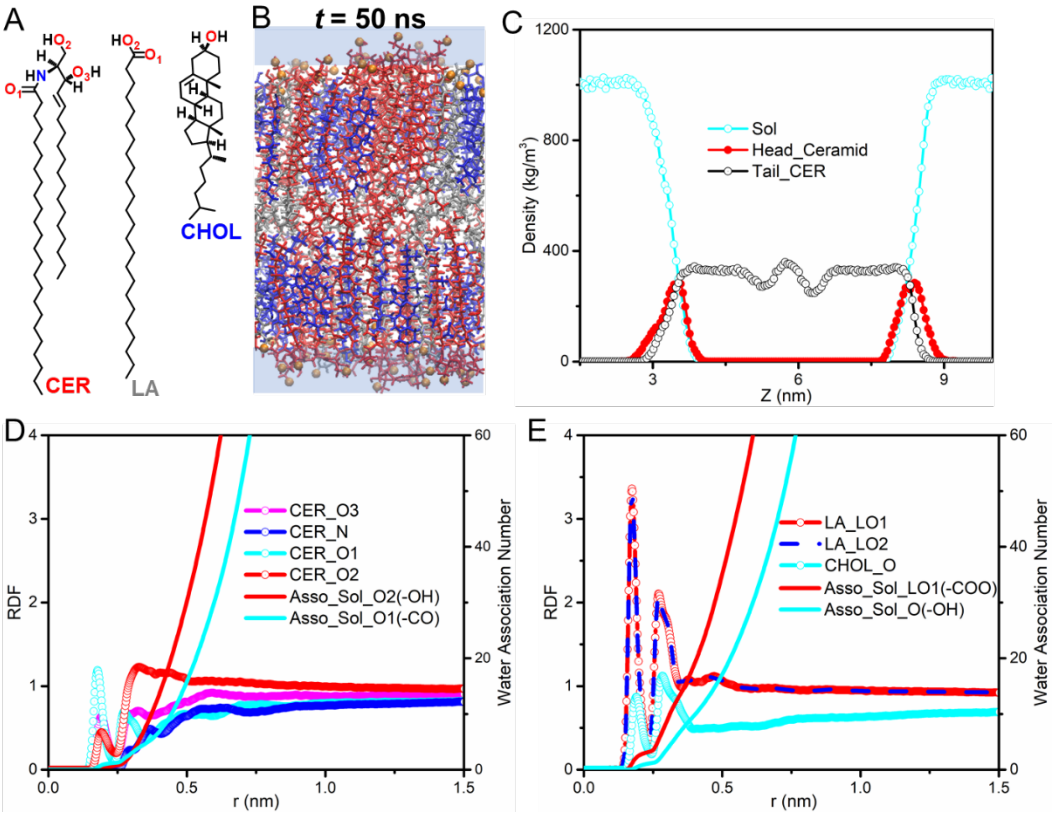

Figure S8. A) Chemical structures of CER, CHOL, lignoceric acid LA. B) Snapshot of CER/CHOL/LA at equimolar ratio at the end of the simulation at the end of 50 ns simulation. CER molecules are shown in red, CHOL in blue, LA in grey, and water as light blue layer. C) Mass density profiles of CER head, tail and solvent. D) RDFs of the selected atoms in CER and the corresponding water association number function. E) RDFs of the selected atoms in LA and CHOL, and the corresponding water association number function.

Table S4. Hydration radius and average water association number for LA and surfactant head in different model membranes.

System name	Hydration layer of negatively charged group (LO1/LO2)		Hydration radius of positively charged group (NC3), association number
	First hydration radius (nm), water association number	Second hydration radius (nm), water association number	
CER^{Pure}	0.24, 3.24	0.35, 13.15	--
CER^{C16HAB}	0.24, 3.07	0.35, 12.39	0.55, 27.76
CER^{IHAB}	0.24, 2.96	0.35, 11.89	0.54, 26.63

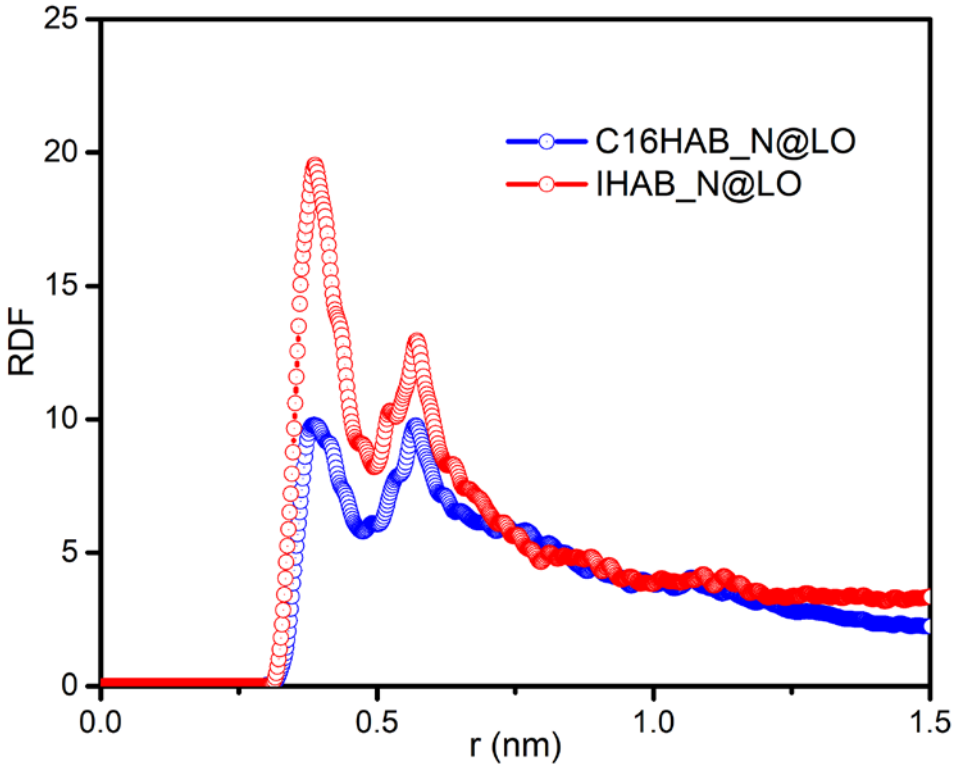

Figure S9. RDFs of the positively charged surfactant head -HAB with negatively charged COO^- group in LA.